©

Det här verket är upphovrättskyddat enligt *Lagen (1960:729) om upphovsrätt till litterära och konstnärliga verk*. Det har digitaliserats med stöd av Kap. 1, 16 § första stycket p 1, för forskningsändamål, och får inte spridas vidare till allmänheten utan upphovsrättsinehavarens medgivande.

Alla tryckta texter är OCR-tolkade till maskinläsbar text. Det betyder att du kan söka och kopiera texten från dokumentet. Vissa äldre dokument med dåligt tryck kan vara svåra att OCR-tolka korrekt vilket medför att den OCR-tolkade texten kan innehålla fel och därför bör man visuellt jämföra med verkets bilder för att avgöra vad som är riktigt.

This work is protected by Swedish Copyright Law (*Lagen (1960:729) om upphovsrätt till litterära och konstnärliga verk)*. It has been digitized with support of Kap. 1, 16 § första stycket p 1, for scientific purpose, and may no be dissiminated to the public without consent of the copyright holder.

All printed texts have been OCR-processed and converted to machine readable text. This means that you can search and copy text from the document. Some early printed books are hard to OCR-process correctly and the text may contain errors, so one should always visually compare it with the images to determine what is correct.

GÖTEBORGS UNIVERSITET
GÖTEBORGS UNIVERSITETSBIBLIOTEK

Imaging Properties of Digital Radiographic Systems

Development, Application and Assessment of Evaluation Methods Based on Linear-Systems Theory

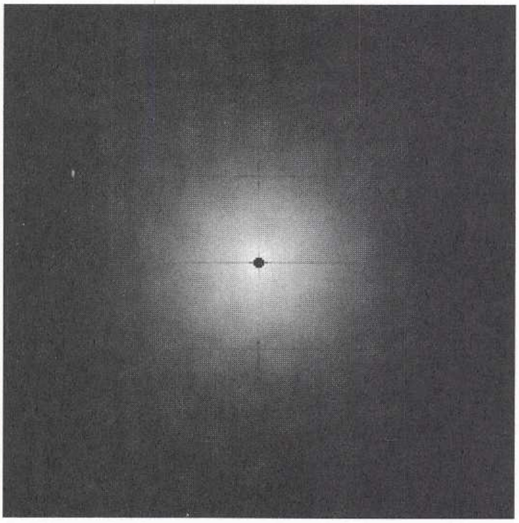

MAGNUS BÅTH

Department of Radiation Physics
Göteborg University

GÖTEBORG UNIVERSITY

1041

Imaging Properties of Digital Radiographic Systems

Development, Application and Assessment of Evaluation Methods Based on Linear-Systems Theory

Magnus Båth
fil. lic.

AKADEMISK AVHANDLING
som för avläggande av filosofie doktorsexamen i radiofysik vid Göteborgs universitet kommer att offentligen försvaras fredagen den 6 juni 2003 kl 9.15 i Föreläsningssal Ivan Ivarsson, Medicinaregatan 3, Medicinareberget, Göteborg

Fakultetsopponent: Docent Mats Nilsson
Avdelningen för radiofysik
Universitetssjukhuset MAS, Malmö

Avdelningen för radiofysik
Göteborgs universitet
Göteborg, 2003

Abstract

Digital radiographic systems are becoming more and more common in projection radiography. These systems are linear or can be linearized, which makes the use of methods based on linear-systems theory appropriate for evaluating the imaging properties. However, the fact that the systems sample the signal at discrete locations may lead to non-stationarity, which demands adaptation of the evaluation methods since these often assume not only linearity but also stationarity. The work described in this thesis was aimed at investigating methods based on linear-systems theory for evaluating the imaging properties of digital radiographic systems through the application of existing methods and the development of new methods, as well as the assessment of these methods – both in terms of the validity and reliability of the results and their importance regarding the clinical performance of the systems.

A computer program for simulating the modulation transfer function (MTF) of a digital radiographic detector was developed. The program simulates a detector using the sampling distance and sampling aperture, and the spread of signal due to the interaction processes of the incoming photons. The program was used to investigate the effects on the MTF of the design of the system. The program was also used to simulate a measurement of the presampling MTF with the slit method, and it was found that the slit could have a finite width and still give valid results.

A new method of determining the two-dimensional presampling MTF – the aperture mask method – was developed. The method is based on imaging an aperture mask, consisting of an array of cylindrical holes drilled in an attenuating material. The image data are used to construct a finely sampled disk spread function (DSF) which can be Fourier transformed and corrected for the finite size of the holes to obtain the two-dimensional presampling MTF. The method was applied to two computed radiography (CR) systems and was found to be consistent with the established tilted slit method in determining the one-dimensional presampling MTF. The method was used to determine the two-dimensional detective quantum efficiency (DQE) of a CR system.

The imaging properties of two generations of a CCD-based digital radiography (DR) system for chest radiography were analysed in detail through experimental determination of the presampling MTF, the noise power spectrum (NPS), the noise equivalent quanta (NEQ) and the DQE, as well as through modelling of the DQE and the production of quantum accounting diagrams (QADs). It was found that the second generation was substantially improved compared with its predecessor regarding all relevant measures, mainly due to a better system gain. However, modelling showed that both systems suffer from low optical efficiency due to the high degree of demagnification employed, leading to a secondary quantum sink and relatively modest DQE for both systems, especially at low exposures.

A study was conducted to compare the imaging properties, mainly in term of DQE, of digital radiographic systems with the clinical image quality, determined using visual grading analysis (VGA) of important anatomical structures, of chest images produced with the systems. It was found that a system with a low DQE could produce images with a clinical image quality comparable to that of systems with substantially higher DQEs. The results indicate that in chest radiography performed at standard dose (speed class 200), quantum noise and system noise do not dominate the clinical image quality but anatomical structure and image processing.

Keywords: linear-systems theory (LST), linear-systems analysis (LSA), digital radiography (DR), computed radiography (CR), digital radiographic systems, detective quantum efficiency (DQE), modulation transfer function (MTF), noise power spectrum (NPS), noise equivalent quanta (NEQ), quantum accounting diagram (QAD), image quality, visual grading analysis (VGA), chest radiography, imaging properties

ISBN 91-628-5651-0

Imaging Properties of Digital Radiographic Systems

Development, Application and Assessment of Evaluation Methods Based on Linear-Systems Theory

Magnus Båth

Department of Radiation Physics
Göteborg University
Göteborg, 2003

Doctoral Thesis, 2003
Department of Radiation Physics
Göteborg University
Göteborg, Sweden

Imaging Properties of Digital Radiographic Systems – Development, Application and Assessment of Evaluation Methods Based on Linear-Systems Theory
Magnus Båth
ISBN 91-628-5651-0

Copyright © Magnus Båth, 2003 (pages 1-94)

Department of Radiation Physics
Göteborg University
Sahlgrenska University Hospital
SE-413 45 Göteborg
SWEDEN

Printed in Sweden by
Vasastadens Bokbinderi AB, Göteborg, 2003

The cover illustration shows the two-dimensional detective quantum efficiency (DQE) of a digital radiographic system. The two-dimensional DQE was determined using a new method for determining two-dimensional imaging properties of digital radiographic systems, the aperture mask method.

"O Fortuna
velut luna
statu variabilis"

From *Carmina Burana* (Carl Orff, 1936)

Abstract

Digital radiographic systems are becoming more and more common in projection radiography. These systems are linear or can be linearized, which makes the use of methods based on linear-systems theory appropriate for evaluating the imaging properties. However, the fact that the systems sample the signal at discrete locations may lead to non-stationarity, which demands adaptation of the evaluation methods since these often assume not only linearity but also stationarity. The work described in this thesis was aimed at investigating methods based on linear-systems theory for evaluating the imaging properties of digital radiographic systems through the application of existing methods and the development of new methods, as well as the assessment of these methods – both in terms of the validity and reliability of the results and their importance regarding the clinical performance of the systems.

A computer program for simulating the modulation transfer function (MTF) of a digital radiographic detector was developed. The program simulates a detector using the sampling distance and sampling aperture, and the spread of signal due to the interaction processes of the incoming photons. The program was used to investigate the effects on the MTF of the design of the system. The program was also used to simulate a measurement of the presampling MTF with the slit method, and it was found that the slit could have a finite width and still give valid results.

A new method of determining the two-dimensional presampling MTF – the aperture mask method – was developed. The method is based on imaging an aperture mask, consisting of an array of cylindrical holes drilled in an attenuating material. The image data are used to construct a finely sampled disk spread function (DSF) which can be Fourier transformed and corrected for the finite size of the holes to obtain the two-dimensional presampling MTF. The method was applied to two computed radiography (CR) systems and was found to be consistent with the established tilted slit method in determining the one-dimensional presampling MTF. The method was used to determine the two-dimensional detective quantum efficiency (DQE) of a CR system.

The imaging properties of two generations of a CCD-based digital radiography (DR) system for chest radiography were analysed in detail through experimental determination of the presampling MTF, the noise power spectrum (NPS), the noise equivalent quanta (NEQ) and the DQE, as well as through modelling of the DQE and the production of quantum accounting diagrams (QADs). It was found that the second generation was substantially improved compared with its predecessor regarding all relevant measures, mainly due to a better system gain. However, modelling showed that both systems suffer from low optical efficiency due to the high degree of demagnification employed, leading to a secondary quantum sink and relatively modest DQE for both systems, especially at low exposures.

A study was conducted to compare the imaging properties, mainly in term of DQE, of digital radiographic systems with the clinical image quality, determined using visual grading analysis (VGA) of important anatomical structures, of chest images produced with the systems. It was found that a system with a low DQE could produce images with a clinical image quality comparable to that of systems with substantially higher DQEs. The results indicate that in chest radiography performed at standard dose (speed class 200), quantum noise and system noise do not dominate the clinical image quality but anatomical structure and image processing.

Keywords: linear-systems theory (LST), linear-systems analysis (LSA), digital radiography (DR), computed radiography (CR), digital radiographic systems, detective quantum efficiency (DQE), modulation transfer function (MTF), noise power spectrum (NPS), noise equivalent quanta (NEQ), quantum accounting diagram (QAD), image quality, visual grading analysis (VGA), chest radiography, imaging properties

List of papers

This thesis is based on the following papers, which will be referred to by their Roman numerals:

I. M. Båth, P. Sund and L. G. Månsson
Investigation of Parameters Concerning the Modulation Transfer Function in Digital Radiography
In *Medical Imaging 2001: Physics of Medical Imaging,* Larry E. Antonuk, Martin J. Yaffe, Editors, Proceedings of SPIE Vol. 4320, 350-361 (2001)

II. M. Båth, P. Sund and L. G. Månsson
Method for Determining the Two-Dimensional Presampling Modulation Transfer Function in Digital Radiography
In *Medical Imaging 2001: Physics of Medical Imaging,* Larry E. Antonuk, Martin J. Yaffe, Editors, Proceedings of SPIE Vol. 4320, 268-279 (2001)

III. M. Båth, M. Håkansson and L. G. Månsson
Determination of the Two-Dimensional Detective Quantum Efficiency of a Computed Radiography System
Submitted 2003

IV. M. Båth, P. Sund and L. G. Månsson
Evaluation of the Imaging Properties of Two Generations of a CCD-based System for Digital Chest Radiography
Med. Phys. **29**, 2286-2297 (2002)

V. P. Sund*, M. Båth*, S. Kheddache and L. G. Månsson
Comparison of Visual Grading Analysis and Determination of Detective Quantum Efficiency for Evaluating System Performance in Digital Chest Radiography
Accepted for publication in *European Radiology* 2003
*Both authors contributed equally to this work

Published papers are reprinted with the kind permission of SPIE – The International Society for Optical Engineering (Papers I and II) and AAPM (American Association of Physicists in Medicine) (Paper IV).

Preliminary reports

- M. Båth, P. Sund and L. G. Månsson
  Development of a Slit and Software for Determining the MTF of a Digital Radiographic System
  Presented at the Sixth Göteborg Graduate School in Biomedicine Symposium, Göteborg, Sweden, January 15, 1999

- P. Sund, M. Båth, S. Kheddache, U. Tylén and L. G. Månsson
  Evaluation of Image Quality of a New CCD-based System for Chest Imaging
  Presented at Medical Imaging 2000: Physics of Medical Imaging, San Diego, USA, February 13-15, 2000

- M. Båth, P. Sund and L. G. Månsson
  Method for Determining the Two-Dimensional Presampling Modulation Transfer Function in Digital Radiography
  Presented at Medical Imaging 2001: Physics of Medical Imaging, San Diego, USA, February 18-20, 2001

- M. Båth, P. Sund and L. G. Månsson
  Investigation of Parameters Concerning the Modulation Transfer Function in Digital Radiography
  Presented at Medical Imaging 2001: Physics of Medical Imaging, San Diego, USA, February 18-20, 2001

Contents

Abbreviations 11

1. Introduction 13

1.1 Background 13
1.2 Digital radiographic systems 13
1.2.1 CR 14
1.2.2 DR 15
1.3 Evaluating system performance 16
1.4 Aims 17

2. Linear-Systems Analysis 19

2.1 Introduction to linear-systems theory 19
2.2 Detective quantum efficiency: presentation of the concept 22
2.3 Modulation transfer function 24
2.3.1 The MTF of an analogue system 24
2.3.2 The MTF of a digital radiographic system 25
2.3.3 Determining the MTF 26
2.3.4 Determining the MTF of a digital radiographic system 28
2.4 Simulating the MTFs of digital radiographic systems (Paper I) 32
2.5 Determining the two-dimensional presampling MTF (Paper II) 35
2.6 Noise power spectrum 40
2.6.1 The NPS of an analogue system 40
2.6.2 The NPS of a digital radiographic system 41
2.6.3 Determining the NPS of a digital radiographic system 41
2.6.4 Obtaining a one-dimensional NPS 43
2.6.5 Normalized NPS 44
2.7 Detective quantum efficiency: expansion of the concept 45
2.7.1 Frequency dependency 45
2.7.2 NEQ 46
2.7.3 The ideal detector and the problem of determining SNR_{in} 46
2.7.4 The DQE of a digital radiographic system 48
2.7.5 Determining the DQE of a digital radiographic system 49
2.7.6 Standardized determination of the DQE 50
2.7.7 Modelling the DQE 50
2.7.8 Uncertainties in DQE determination 51
2.8 Determining the two-dimensional DQE (Paper III) 52
2.9 Evaluation of two generations of a CCD-based DR system (Paper IV) 57

3. Clinical System Performance 63

3.1 Operationalization – or: What was actually measured? 63
3.2 Evaluation of image quality 64
3.2.1 An introductory example and a global concept of image quality....................64
3.2.2 Grading of visibility of details...65
3.2.3 The CEC quality criteria...67
3.2.4 Weaknesses of VGA...68
3.3 Comparison of DQE and VGA (Paper V) 69

4. Summary and Conclusions 75

5. Concluding Remarks and Future Prospects 77

Acknowledgements 79

References 81

Abbreviations

AEC	automatic exposure control
ALARA	as low as reasonably achievable
ANOVA	analysis of variance
BIPM	Bureau International des Poids et Mesures
CCD	charge-coupled device
CEC	Commission of the European Communities
CR	computed radiography
CT	computed tomography
DFT	discrete FT
DR	digital radiography
DSF	disk spread function
DQE	detective quantum efficiency
EMTF	expectation MTF
ESF	edge spread function
ERF	edge response function
FFE	free-response forced error
FPD	flat panel detector
FFT	fast FT
FT	Fourier transform
FWHM	full width at half maximum
ICS	image criteria score
IEC	International Electrotechnical Commission
IQI	image quality index
IRF	impulse response function
K_{air}	entrance air kerma free in air
LSA	linear-systems analysis
LSF	line spread function
LST	linear-systems theory
MRI	magnetic resonance imaging
MTF	modulation transfer function
MTF_d	digital MTF
MTF_{max}	maximum MTF
MTF_{min}	minimum MTF
MTF_{pre}	presampling MTF
MTF_S	sampling aperture MTF
NEQ	noise equivalent quanta
NNPS	normalized NPS
NPS	noise power spectrum
NPS_A	analogue input NPS
NPS_d	digital NPS

OTF	optical transfer function
OTF_A	analogue input OTF
OTF_d	digital OTF
OTF_S	sampling aperture OTF
PA	posterior-anterior
PMMA	poly(methyl methacrylate)
PSF	point spread function
QAD	quantum accounting diagram
RQE	responsive quantum efficiency
ROC	receiver operating characteristics
ROI	region of interest
SNR	signal-to-noise ratio
SWRF	square-wave response function
T	characteristic function
TFT	thin-film transistor
VGA	visual grading analysis
VGAS	VGA score
$VGAS_{abs}$	absolute VGAS
$VGAS_{rel}$	relative VGAS

1. Introduction

1.1 Background

The discovery of X-rays in 1895 and their ability to penetrate opaque materials had an immediate impact on medicine. X-rays were used perfunctionarily to image the interior of the human body already at the end of the 19th century [1]. In the beginning, planar X-ray imaging – mapping of an object onto a two-dimensional image using an X-ray source and an imaging detector – was used. Later, new ways of using X-rays for diagnostic imaging were invented, *e.g.* computed tomography (CT), which results in a three-dimensional representation of the imaged object. However, planar imaging is still the most common application of X-rays in medicine.

The contrast in an X-ray image is caused by differences in attenuation in the imaged object. The attenuation transfers energy to the object. Since X-rays are ionizing radiation, a radiation dose is thus received by the object being imaged with X-rays. For humans and other living creatures, this radiation dose is associated with a stochastic risk of inducing cancer. It is therefore of the utmost importance that the radiation dose be kept as low as possible – by not using more radiation than is necessary to produce an image with sufficient quality for the specific task (generally, the more X-ray photons used to form the image, the smaller the effect of quantum noise in the image) – in accordance with the ALARA (as low as reasonably achievable) principle [2]. In order to accomplish this, the imaging procedure has to be optimized. Over the years, there has therefore been considerable scientific interest in characterizing the imaging properties of imaging detectors as well as the quality of the images produced with these detectors, and a great deal of work has been carried out in this field. The transition to using digital radiographic detectors requires increased effort in the medical imaging community since the properties of digital detectors demand adaptation of methods used to evaluate analogue systems; these methods being inadequate for digital systems. The work described in thesis is a continuation of the work to develop methods of characterizing and evaluating digital radiographic systems.

1.2 Digital radiographic systems

For many years, screen/film systems dominated radiography. An X-ray film has the advantage that it is simultaneously a detection, storage and display medium. However, major drawbacks of an analogue film are that the final image cannot be further processed and that the dose response is limited. In later years, several different digital radiographic systems have therefore been developed. Since these produce images in digital form, the images can be processed in order to achieve the desired contrast and resolution. The image can then either be displayed on a monitor (soft-copy reporting) or printed on a film (hard-copy reporting). Digital radiographic systems also often have wider latitude, meaning that the risk of under- or overexposing images is smaller. Digital radiographic systems can be classified in different ways. Today, most systems belong either to computed radiography (CR) or to digital radiography (DR). Whereas all CR systems bear great resemblance to each other, the DR family consists of systems with large differences, connected only by the fact that the X-rays are converted into an electric signal which is immediately used to create an image. A short presentation of CR and DR will be given here. First, however, clarification of DR will be given. The term 'digital radiography' has with time gained an ambiguous meaning. It has sometimes been used to describe all types of digital radiographic systems [3-5]. However, it has in recent years come to be used to describe only those imaging systems that contain integrated readout mechanisms, which excludes CR [6]. As guidance, when the term digital radiography is used non-abbreviated this usually implies the former meaning – especially in older publications, whereas when it is used in its abbreviated form (DR), especially in the combination 'DR system', CR systems are usually excluded. In this thesis, an effort has been made to reduce the risk of confusion by using the term 'digital radiographic system' as far as possible to describe a planar X-ray imaging system resulting in digital images. Unfortunately, in some of the papers 'digital radiography' is used with this meaning. Hopefully, the context makes the meaning clear.

1.2.1 CR

Storage-phosphor systems, often referred to as computed radiography (CR), use the principle of photostimulated luminescence [7], which means that a material stores part of the energy of the incoming X-rays and releases it later during irradiation with by. By adding a phosphor layer to a supporting material, a so-called image plate is obtained. The image plate resembles an analogue X-ray film regarding size and usage as a detector for X-rays. The greatest difference is that while X-ray film is also the storage medium and means of displaying the image, the information on the image plate is transferred to a computer, where it is stored. This is done in the readout process, during which the image plate is exposed to a laser beam which sweeps over the plate. During laser irradiation, the image plate emits light, which is collected and digitized, resulting in a digital representation of the spatial radiation intensity pattern. The direction in which the laser beam sweeps is usually called the 'scan' or 'fast scan' direction, whereas the orthogonal direction, in which the image plate is slowly transported during the readout process, is called the 'subscan' or 'slow scan' direction. The technique was first proposed in 1983 [8], and led to a commercial system from Fuji (Tokyo, Japan). Later, Agfa-Gevaert (Mortsel, Belgium), Kodak (Rochester, NY, USA) and Konica (Tokyo, Japan) developed their own systems for CR. Other companies, such as Philips (Hamburg, Germany) and Siemens (Erlangen, Germany), use components from the above mentioned manufacturers, but produce their own CR systems. CR was the first digital radiographic system to seriously compete with screen/film, and is still the leading digital alternative. An extensive review of the physics of CR, including its fundamental limitations and possibilities for improvement, was recently presented by Rowlands [9].

1.2.2 DR

DR covers a more heterogeneous group of imaging detectors than CR, and consists of several different subgroups. An important one, consisting of flat-panel detectors (FPDs), has gained increasing interest in recent years due to its extremely high intrinsic resolution [10] and absorptive properties [11,12]. An FPD, although technically complicated, basically consists of a converting layer deposited on a large-area thin-film transistor (TFT) array [6]. This construction enables the charge collection and readout electronics for each pixel to be situated at the location of the photon interaction, which makes the use of optical coupling unnecessary. This leads to the possibility of combining high detection efficiency with a small signal spread in the detector.

The FPDs can be separated into two classes, depending on whether direct or indirect methods are used to convert the X-rays into electric charges in the TFT array.

1) FPDs using direct methods make use of a converting layer of an X-ray photoconducting material. These materials have the property that they become conductive when exposed to ionizing radiation, and this is used to collect the charges that are released when the detector is irradiated. The so far most successfully used material is amorphous selenium (a-Se) [13-15]. However, other materials such as PbI_2 [16], HgI_2 [17], CdTe [18] and CdZnTe [19] have been investigated.

2) FPDs using indirect detection employ a scintillating material like CsI(Tl) [20,21] or Gd_2O_2S(Tb) [22] to convert the X-rays to light. The light is thereafter converted to electric charge using a large-area photodiode array.

Another subgroup within DR is made up of systems based on the CCD (charge-coupled device) technique – an integrated circuit basically consisting of an array of small photodiodes. Such a system uses a scintillating screen to convert the X-rays to light. The light is then transported to a CCD camera, either by an optical system of lenses and mirrors [23] or by fibre optics [24], where it is converted to electric signals. The technique is simple, but suffers from the fact that CCDs cannot easily be made large [25]. Demagnification must therefore be used to match the true size of the image to the CCD, which decreases the light collection efficiency [26]. CCD-based detectors have therefore mainly been used in mammography [24,27,28], where the demagnification can be kept small due to the small imaging area.

A specific CCD-based DR system of importance in the present work has been manufactured by IMIX ADR Oy (Tampere, Finland). This system uses mirrors and lenses to reflect and refract the light emitted by the scintillating screen to match the sensitive area of the CCD camera. A 'black map' is used to remove unwanted bias due to the CCD camera from the signal (offset correction) and a 'bright map' is applied to correct for pixel-to-pixel variation in sensitivity (gain correction). The signal is sent through an acquisition computer to the control station, where the image is processed. The first generation of detectors was named IMIX and the second version was called IMIX 2000. The IMIX was released in the mid 1990s and had a scintillating screen made of $Gd_2O_2S(Tb)$. This screen emits light in the green part of the spectrum, while the CCD used is more sensitive to red light. The second generation of this system, the IMIX 2000, was therefore equipped with a screen of $Gd_2O_2S(Eu)$, which emits red light, to better match the sensitivity of the CCD. The optics was also upgraded with a new mirror system and a new lens. The thorax versions of both systems, which were used in this work, use a demagnification of 13.3, a pixel size of 200 μm and a total field size of 40x40 cm^2.

1.3 Evaluating system performance

The requirements of an imaging system and the demands on the image quality are dependent on the imaging task. However, a desire to describe the imaging properties of an imaging system in an objective way, without taking the specific imaging task into account, has led to the application of linear-systems analysis (LSA) to medical imaging systems. LSA, based on linear-systems theory (LST) [29], can be used to give measures of the ability of the system to pass a signal, as well as of the noise characteristics of the system. The reasoning behind the use of LSA is to give general and detailed descriptions of the imaging system in terms of properties that are believed to influence the system performance. A completely different approach is to evaluate the quality of images collected with the system by allowing a human observer to rate the visibility of specific details in the image. The output of the observer, when the image produced by the system is the input, is used to evaluate the image, and thus also the system. Of special interest in the present work is visual grading analysis (VGA) of anatomical structures in clinical images, based on the assumption that the visibility of anatomy is correlated to the detection of pathology. The resulting measure of image quality is intended to describe the clinical performance of a system.

Both methods of evaluating system performance have been widely used. LSA usually incorporates determination of quantities such as the modulation transfer function (MTF) – describing the signal spread in the system, the noise power spectrum (NPS) – giving a detailed description of the noise in the system – and the detective quantum efficiency (DQE) – describing the efficiency of the system in transferring information. Such evaluations have been performed on storage-phosphor systems [30-41], flat-panel detectors [10,13,42-46] and CCD-based systems [28]. Investigations of this kind are most often performed shortly after a new system becomes available on the market. Theoretical investigations of the mentioned quantities are also common [11,26,47,48], and are sometimes used in the development stage of new imaging systems. Evaluations of the clinical image quality have been performed frequently in both digital and screen/film radiography [23,49-53], and are often used when trying to optimize existing equipment.

The two above-mentioned methods constitute only some of the approaches used to determine system performance, but are the only ones applied in the present work. Numerous other methods can be found in the literature [54,55], and among them of interest today are ROC-related (receiver operating characteristics) methods [56-59] – studying the ability of human observers to detect a signal in an image – and methods incorporating model observers [60-62] – using a mathematical model to describe the ability of observers to detect a signal in an image. Subjective measures of physical quantities, *e.g.* using contrast-detail diagrams to determine detectability and bar-patterns to determine the resolution, can also be used.

1.4 Aims

The overall aim of this work was to develop, apply and assess methods based on LST for evaluation of the imaging properties of digital radiographic systems. The specific aims were:

- to develop a computer program simulating the resolution properties, in terms of different MTFs, of hypothetical imaging detectors and to evaluate the influence of some design parameters on the resulting MTFs (Paper I),

- to develop methods for determining the imaging properties of digital radiographic systems in terms of the two-dimensional presampling MTF and the two-dimensional DQE (Papers II and III),

- to evaluate the imaging properties of a CCD-based DR system through experimental and theoretical LSA (Papers IV and V) and

- to investigate the relationship between the imaging properties of digital radiographic systems and the clinical image quality in order to assess the validity of DQE as a measure of clinical system performance in digital chest radiography (Paper V).

An important aim was also to explain why, how, and with what limitations methods based on LST can be used to evaluate the performance of digital radiographic systems. This thesis is therefore arranged in the following way. The first part covers the foundation for, development of and application of methods based on LST for evaluating the imaging properties or physical system performance of digital radiographic systems. In the second part, methods of determining the clinical image quality are introduced and LSA is assessed as a method for evaluating clinical system performance. Details on and experience gained from the studies described in the papers on which this thesis is based are presented throughout the text. A separate section is also devoted to each paper where the study is described in more detail.

2. Linear-Systems Analysis

2.1 Introduction to linear-systems theory

In order to characterize the input/output relationship of a system, without any assumptions being made on the properties of the system, extensive measurements would be needed. The response to each unique signal would be unknown, leading to an infinite amount of combinations to be tested. If the system is represented by an operator S{ } acting on an input f(x,y) to produce an output g(x,y), then the relationship between f(x,y) and g(x,y) cannot be described in more detail than:

$$g(x,y) = S\{f(x,y)\}. \tag{2.1}$$

However, if the system is *linear* it is possible to use the response of the system to a set of elementary inputs to predict the response to any input [63]. A system is linear if and only if it obeys the rules of *additivity* and *homogeneity*, *i.e.* if a system has a transfer characteristic S{ } such that the response of the system to a signal f(x,y) is S{f(x,y)}, then the system is linear if and only if the relationships:

$$S\{f_1(x,y) + f_2(x,y)\} = S\{f_1(x,y)\} + S\{f_2(x,y)\}, \tag{2.2}$$

and

$$S\{af(x,y)\} = aS\{f(x,y)\}, \tag{2.3}$$

where a is a constant, hold [29]. No real systems are truly linear, meaning that the linear-systems approach is an approximation. However, for many systems the approximation is justified, especially for small signals [29]. Linear-systems theory is also applied to systems that are not linear but can be linearized through the use of mathematical transformations. An example of such a system is a CR system for which the output is usually logarithmic or square-root compressed.

For a linear system, Eq. (2.1) can be transformed into the following equation [63]:

$$g(x,y) = \int_{-\infty}^{\infty}\int_{-\infty}^{\infty} f(x_1,y_1)h(x,y;x_1,y_1)dx_1dy_1 \; . \tag{2.4}$$

In Eq. (2.4), $h(x,y;x_1,y_1)$ is the response of the system at the output coordinate (x,y) to a delta function input at (x_1,y_1). Although Eq. (2.4) appears ostensibly to be more complicated than Eq. (2.1), the restriction that the system is linear leads to considerable simplification of the description of the input/output relationship: a linear system is completely specified by its response to a delta function input. This response, described by the function h(x,y;x_1,y_1), is called the impulse response function (IRF) or, more commonly for imaging systems, the point spread function (PSF) [29].

The description of the system can be simplified further if it is assumed that the system is *stationary*. For a stationary system, the PSF is only dependent on the difference (x-x_1,y-y_1) and not on each variable separately, meaning that the response of the system to a signal is the same at all locations [63]. Such a system is therefore also called *shift invariant* [29]. A linear *and* stationary imaging system is therefore not only completely specified by its response to a delta function input, but this response is the same over the whole imaging detector, leading to the reduction of Eq. (2.4) to [63]:

$$g(x,y)=\int_{-\infty}^{\infty}\int_{-\infty}^{\infty}f(x_1,y_1)h(x-x_1,y-y_1)dx_1dy_1\,. \tag{2.5}$$

The right-hand term of Eq. (2.5) can be identified as the convolution of the functions f and h, and for an imaging system this is usually presented in the following form:

$$g(x,y) = f(x,y)\otimes PSF(x,y)\,, \tag{2.6}$$

where the symbol ⊗ represents the convolution operator. The output of a linear and stationary system in response to an arbitrary input is therefore simply a convolution of the input with the PSF of the system.

For a linear, stationary system, the Fourier transform may be used to advantage to describe the properties of the system. The two-dimensional Fourier transform F(u,v) of the function f(x,y) is given by [63]:

$$F(u,v)=\int_{-\infty}^{+\infty}\int_{-\infty}^{+\infty}f(x,y)e^{-2\pi i(ux+vy)}dxdy\,. \tag{2.7}$$

F(u,v) and f(x, y) are said to be a Fourier transform pair and the units of their variables are the reciprocal of each others. Examples of variables are time (s) and temporal frequency (Hz), and, as used in the present work, distance (mm) and spatial frequency (cycles/mm or mm^{-1}). A shorter notation of F(u,v) as the Fourier transform (FT) of f(x,y), which will be used in this thesis, is:

$$F(u,v)=FT\{f(x,y)\}. \tag{2.8}$$

The Fourier transform provides a means of moving between two domains, giving the same information in two different ways. By Fourier transforming an image a representation of the spatial frequencies the image is composed of is obtained. The reason for using the Fourier transform is that the information may be easier to interpret in one or the other domain. Another reason for using the Fourier transform is that it has some appealing properties; the one that states that convolution in one domain corresponds to multiplication in the other is used frequently in LSA. This can be used to transform Eq. (2.6) into:

$$G(u,v) = F(u,v)T(u,v)\,, \tag{2.9}$$

where T is the characteristic function of the system, given by the Fourier transform of the PSF [29]. For a stationary linear system, the output frequency spectrum is therefore completely described by multiplication of the input spectrum by the characteristic function. If the characteristic function is normalized to unity at zero frequency, the optical transfer function (OTF) is obtained [29]. Often, however, it is assumed that the PSF is already normalized in such a way that the zero-frequency value of the characteristic function is unity, in which case the OTF equals the characteristic function.

When applied to digital data, a discrete Fourier transform (DFT) is used. The DFT is, as the name implies, the digital analogue to the Fourier transform, which is applied to continuous data. Specifically, a fast Fourier transform (FFT) is generally used to perform the specific calculations. Different FFTs exist, and they can be scaled in different ways [29]. However, in the present work the expression 'Fourier transform' will be used for discrete as well as continuous Fourier transforms.

Based on LST and the use of the Fourier transform, a number of quantities have been developed to describe the imaging properties of radiographic detector systems. These frequency-dependent quantities replace more diffuse measures such as resolution, sharpness and uniformity. Among these quantities are the MTF, describing the contrast reduction of the different spatial frequencies, and the NPS, describing the frequency components of the noise. These quantities can be used to determine the NEQ, describing the square of the signal-to-noise ratio (SNR) of different frequencies in the image, and the DQE, describing the ability of the system to transfer the squared SNR from the input stage to the output stage. These quantities will be explained and discussed below.

Closely related to the Fourier transform are the Nyquist frequency and the concept of aliasing. For a system that samples the incoming signal at discrete locations, the Nyquist frequency describes the highest frequency that can be correctly transferred by the system. The Nyquist frequency is given by half the sampling frequency [64]. (For a two-dimensional sampling system such as a digital radiographic system, the sampling frequency is different in different directions. However, it is usually stated along a coordinate axis where it is equal to the inverse of the pixel size. A system with a pixel size of 0.2 mm is therefore attributed a Nyquist frequency of 2.5 mm^{-1}. The term 'pixel size' can be found with different meanings, but is used here to describe the distance between the sampling points along a coordinate axis.) An input to the system of a frequency higher than the Nyquist frequency will take the form of a different frequency at the output, hence the term aliasing (Fig. 2.1). This matter is of interest for digital radiographic systems, since the discrete nature of the pixels leads to aliasing if the sampling system is not matched to the signal, *i.e.* if the sampling distance is not small enough to correctly sample all incoming frequencies. An undersampled system is not stationary, meaning that the response of an undersampled digital system is dependent on the position of the signal. The effects of the non-stationarity of undersampled digital systems on the quantities mentioned above will also be discussed in this thesis.

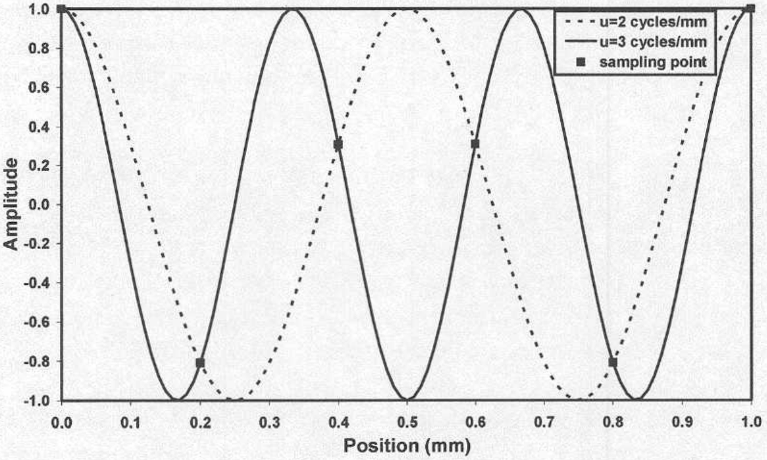

Figure 2.1. The origin of aliasing. A system with a sampling distance of 0.2 mm – resulting in a Nyquist frequency (u_N) of 2.5 mm^{-1} – is exposed to a signal with frequency u=3 mm^{-1}. The sampled points cannot be distinguished from those belonging to a signal with the frequency 2 mm^{-1}. The signal with frequency 3 mm^{-1} therefore takes the alias of a signal with frequency 2 mm^{-1}. Generally, a signal with frequency $u=(i-1)u_N+u_0$ mm^{-1} (for i odd) or $u=iu_N-u_0$ mm^{-1} (for i even) takes the alias of a signal with frequency u_0 mm^{-1} ($0<u_0<u_N$) [65].

2.2 Detective quantum efficiency: presentation of the concept

Since the 1940s, many attempts have been made to quantify the efficiency of radiation detectors [63]. In the first attempts the quantum efficiency was based on the ratio of the number of output events to the number of input events, and was termed the responsive quantum efficiency (RQE). However, the RQE has several drawbacks, the major one being that it "links the input/output numbers in quantity but not in quality" [63]. Amplification anywhere along the signal chain increases the RQE by a proportional amount, which leads to the fact that the RQE does not have an upper limit. It is therefore impossible to compare a real detector with an ideal one in order to obtain an absolute quality measure. However, by comparing the *fluctuations* at the output stage to those at the input stage, a measure with an upper limit of unity is obtained for a linear system. Based on the ratio of fluctuations, the detective quantum efficiency (DQE) can be defined as [63]:

$$DQE = \frac{SNR_{out}^2}{SNR_{in}^2}. \tag{2.10}$$

where SNR_{out} is the signal-to-noise ratio at the output stage and SNR_{in} that at the input stage. The DQE is as such closely connected to the quantum nature of radiation. A measurement of radiation is always associated with an uncertainty, but by comparing the SNR at the output and input stages, the inherent fluctuations of the radiation are excluded from the characterization of the detector, and the detector is compared with an ideal detector – a detector which detects all incoming quanta without adding any noise to the signal. Since ideal amplification – amplification that does not add any noise – increases the noise by the same amount as the signal, the DQE is unaffected by such an amplification stage. However, since no analogue amplification is ideal, an analogue amplification stage decreases the DQE due to the addition of noise. (See Section 2.7.7.)

For any photon-counting detector, not necessarily an imaging detector, the DQE defined according to Eq. (2.10) can be interpreted as the proportion of the available quanta an ideal detector would need to give the same relative uncertainty at the output stage or to give the same SNR of the measurement. Equation (2.10) can therefore be presented in the following way [66]:

$$DQE = \frac{NEQ}{N} \tag{2.11}$$

where N – the number of available quanta – is equal to SNR_{in}^2 due to the Poisson distribution of the quanta and NEQ – the noise-equivalent (number of) quanta – can be interpreted as the number of available quanta an ideal detector would need to give the same relative uncertainty in the measurement. As a simple example, imagine that a non-ideal detector that counts photons has a DQE of 25% and that this detector is exposed to an expected number of 400 photons. For an ideal detector, the only uncertainty in the determination of the number of quanta in the photon field would arise from the quantum nature of the photons which, due to the Poisson distribution of the quanta, results in a standard deviation of $\sqrt{400}=20$. The relative uncertainty for an ideal detector would therefore be 5%. For the non-ideal detector, the average NEQ of this measurement would be $0.25 \cdot 400=100$. This means two things.

1) If repeated measurements were to be made, the standard deviation of the measurement would be √100=10, meaning that the relative uncertainty in the measurement would be 10% instead of the 5% due to the quantum nature of the photons.

2) An ideal detector would give the same relative uncertainty when exposed to an expected number of only 100 quanta. The NEQ can therefore be interpreted as the number of quanta the detected signal 'is worth'.

Note that the DQE is only an interpretation used to visualize the properties of a detector. It does not mean that the detector in the example actually detects, on average, 1 of 4 photons, although it could mean this. It might detect them all. As a matter of fact, if two detectors were to be compared, the detector that detects the highest amount of the photons is not necessarily the detector with the highest DQE since the actual detection of a photon – the stage at which a photon transfers energy to the detector – is only the first stage in the detector. Every new stage that involves stochastic amplification results in a lowering of the DQE, not only due to additive noise, which may not be present, but due to the uncertainty in the amplification. This will be discussed further in Section 2.7.7.

For an imaging detector Eq. (2.11) is usually presented with the right-hand terms expressed per unit area. N is then replaced by the photon fluence, Φ. However, the DQE concept is the same and leads to the interpretation of NEQ as the number of quanta the image 'is worth' per unit area.

2.3 Modulation transfer function

2.3.1 The MTF of an analogue system

For a linear system, the modulation transfer function (MTF) is defined as the ratio of the output modulation to the input modulation of a sinusoidal signal, s, with frequency value (u,v),

$$MTF(u,v) = \frac{M(u,v)_{out}}{M(u,v)_{in}}, \tag{2.12}$$

where the modulation, M, is defined as the ratio of the amplitude of the signal to the average of the signal,

$$M(u,v) = \frac{\frac{1}{2}\left(|s_{\max}| - |s_{\min}|\right)}{\frac{1}{2}\left(|s_{\max}| + |s_{\min}|\right)}. \tag{2.13}$$

For an imaging system, the MTF describes the reduction in contrast of a spatial frequency due to its transport through the system.

The MTF can also be expressed as [66]:

$$MTF(u,v) = |OTF(u,v)|, \tag{2.14}$$

i.e. the modulus of the OTF. The two definitions of the MTF are identical, as is the reasoning behind them. This can be understood by considering the delta function, which is composed of equal amounts of all frequencies. Hence, by presenting a delta function to the system, equal amounts of all frequencies are given as input to the system. By Fourier transforming the response, a representation of the output of the system in the frequency domain is obtained, and the MTF defined according to Eq. (2.14) gives the relative amplitudes of all frequencies at output. This means that imaging a delta function and using Eq. (2.14) to obtain the MTF gives the same result as imaging all frequencies, separately, and using Eq. (2.12) [66]. A formal proof of this equality has been given by Dainty and Shaw in the one-dimensional case [63].

The OTF is a complete descriptor of the transfer of a specific frequency through a system, giving not only information on the modulation modification, but also the phase shift of the frequencies. Although this information may be important, especially when aliasing is a matter for consideration, the MTF is often sufficient to describe the signal transfer through a system.

2.3.2 The MTF of a digital radiographic system

There is one constraint on the equality of the two definitions of the MTF given by Eqs. (2.12) and (2.14). Since, when using Eq. (2.14), all frequencies are given as input to the system simultaneously, the system must be able to separate the frequencies from each other. However, as was mentioned in Section 2.1, aliasing may occur in a sampling system. This phenomenon arises because sampling of a signal will result in replication of the original frequency spectrum of the signal. The replicated spectra are then added over the entire frequency domain, at distances of twice the Nyquist frequency in each direction [3]. In the case of undersampling, the spectra contain frequencies higher than the Nyquist frequency, which results in an overlap of frequency components. The frequencies above the Nyquist frequency will then appear as 'ghost' frequencies below the Nyquist frequency (Fig. 2.1). Since such a frequency cannot be separated from an original frequency component with the same frequency value, the response of the system to a delta function can no longer be used to determine the modulation modification of single frequencies passing through the system [65]. The response of the system will, in this case, be dependent on the phase of the input signal relative to the sampling coordinates. This will be the case if the blurring before the sampling stage is not made large enough to ensure that the amplitudes of the frequencies above the Nyquist frequency are negligible. The digital

MTF (MTF_d) – the sampled MTF obtained from Eq. (2.14) for a digital system – is therefore dependent on the phase of the input signal. This phase-dependency is a violation of the demand for a stationary system, with the result that it is much more difficult to describe the system: Eq. (2.4) cannot be transformed into Eq. (2.6).

A formulation of the digital OTF (OTF_d), derived from Giger and Doi [3] and Dobbins [65] and, in effect, identical to that presented by Fujita *et al.* [67], which was used in Paper I is:

$$OTF_d(u,v;a,b) = OTF_A(u,v)OTF_S(u,v)e^{-2\pi i(ua+vb)} \otimes \sum_{m=-\infty}^{\infty}\sum_{n=-\infty}^{\infty}\delta(u-\frac{m}{\Delta x},v-\frac{n}{\Delta y}), \quad (2.15)$$

where ⊗ denotes convolution, OTF_A is the analogue input OTF including the signal spread in the detector due to the interaction processes and OTF_S is the OTF of the sampling aperture. The $e^{-2\pi i(ua+vb)}$ component represents the effect of the shifts a and b of the signal relative to the sampling coordinates in the x- and y-directions, respectively. Finally, the convolution with the two-dimensional 'bed of nails' in the frequency domain is due to the discrete sampling at distances Δx and Δy in the x- and y-directions, respectively. As can be seen from Eq. (2.15), the effects of sampling can be separated from the analogue components, and the term 'presampling OTF' is used for the product of OTF_A and OTF_S. The corresponding MTF – the presampling MTF (MTF_{pre}) – has become an accepted measure of the signal transfer for digital radiographic systems. Since the presampling MTF is the MTF of the system up to the actual point of sampling, it is not dependent on the phase of the signal and therefore a more appealing description than the MTF_d. Also, the presampling MTF gives the modulation modification of single frequencies passing through the system, even if there is undersampling [65]. Furthermore, the presampling MTF is equal to the MTF_d if there is no undersampling [66].

2.3.3 *Determining the MTF*

When determining the MTF, the one-dimensional MTF is most often used. The one-dimensional MTF is defined as [63]:

$$MTF(u) = \left|FT\{LSF(x)\}\right|, \quad (2.16)$$

where the LSF (line spread function) is the response of a system to a delta function, integrated in the direction opposite to that of concern, and normalized to unity area [29]. It is also the normalized response of a system to a 'line' delta function [29], which is very useful when measuring the one-dimensional MTF. The reason for using the one-dimensional MTF when measuring the MTF is simplicity. In addition, if there is rotational symmetry in system, the one-dimensional MTF, which represents a section of two-dimensional MTF through the origin, completely defines the two-dimensional MTF [63].

A number of methods exist for determining the one-dimensional MTF of a radiographic system. Three commonly used methods are the slit method [68], the edge method [63] and the square-wave response function (SWRF) method [69]. (A fourth method, not commonly used in projection radiography, is the wire method, in which a radio-opaque wire is imaged in order to obtain an 'inverted' LSF [70].)

1) The slit method uses a long, narrow slit (compared with the width of the LSF), placed in the radiation field, to produce an approximate 'line' delta function of X-rays. The response of the system is the LSF convoluted with the beam profile of the slit. Since convolution in the spatial domain corresponds to multiplication in the frequency domain, the modulus of the Fourier transform of the linearized response can be corrected for the narrow slit width in order to obtain the MTF. This is done by division by a sinc function, corresponding to the Fourier transform of the rect-function-shaped beam profile [33]. An alternative to the use of a slit with parallel jaws for the slit method was proposed by Bradford *et al.* [71], who used a standard slit camera with bevelled jaws. The bevelled jaws substantially reduced the alignment sensitivity, although a small residual error was observed after the correction for transmission through the jaws.

2) The edge method is similar to the slit method in that the LSF is determined and used to obtain the MTF. Using this method, a sharp edge is imaged instead of a slit. The response of the system to the sharp edge is the edge spread function (ESF). (The term 'edge response function' – ERF – is also used.) The LSF is then given by the differential of the ESF [63,72] whereupon the MTF can be obtained as above.

With both the slit method and the edge method, the alignment of the device (slit or edge) to the X-ray beam is crucial. The positioning of the slit is demanding due to the very narrow opening. Once penetration is obtained, however, the result is a satisfactory slit image. It is easier to obtain results with the edge method, although it is more difficult to verify that the edge is aligned with the X-ray beam [66].

3) The third method is the SWRF method, which differs substantially from the other two. With this method, a periodic lead-bar pattern is imaged. The lead-bar pattern results in a radiation pattern of different square waves when irradiated. Since a square wave is composed of a basic sinusoid and its harmonics, the basic sinusoid can be described by a number of square waves [69]. By using the responses from the different square waves of the lead-bar pattern, MTF values at certain frequencies can be obtained.

Cunningham and Reid [70] performed a theoretical investigation of the uncertainties in the results from the slit, edge and wire techniques from quantum noise and detector noise. They found that the wire method could never give a better result than the slit method, and that the edge method is preferable for determining the MTF at low frequencies, whereas the slit method is better at high frequencies. However, an experimental comparison between the slit method and the edge method showed good agreement between the two methods [73]. A multi-institutional study of MTF determinations with the slit method and the SWRF method also showed that the variation between these two methods was within the variation expected from interlaboratory comparisons [74].

The MTF concept has been applied to many different medical imaging systems, not only projection radiography. It has been used in such different diagnostic fields as nuclear medicine [75,76], CT [77] and magnetic resonance imaging (MRI) [78], and also in portal imaging in radiation therapy [79,80].

2.3.4 Determining the MTF of a digital radiographic system

Due to aliasing – the false introduction of frequency components due to undersampling – none of the above mentioned methods can be used to determine the one-dimensional MTF of an undersampled digital system without modification. Since aliasing introduces phase dependency, the measured MTF would vary with the location of the imaged object – slit, edge, lead-bar pattern, or wire – relative to the sampling coordinates. In early work on digital radiographic systems, however, the methods were used without modifications. Hillen *et al.* [30] and Papin and Huang [81] applied the SWRF and edge methods, respectively, in their original versions. There was much concern regarding the MTF of digital radiographic systems in the 1980s however, and several methods for determining a one-dimensional presampling MTF were proposed. Two methods that relied on the presampling MTF being zero above twice the Nyquist frequency were described by Sones and Barnes [82] and Fujita *et al.* [83]. The former described a method based on imaging an array of parallel wires, which results in a discrete frequency spectrum that enables the determination of the presampling MTF up to twice the Nyquist frequency through the aliased components. The latter used the average of the digital OTFs obtained from the central and shifted alignment of a slit, also to obtain the presampling MTF up to the twice the Nyquist frequency. Although at least the latter method was applied [31], it was another method based on a simple modification of the slit method that led to a widely accepted method for determining the one-dimensional presampling MTF. Fujita *et al.* [4] proposed a method in which the slit is imaged slightly tilted relative to the axes of the sampling system. Data from several rows are then used to construct a finely sampled LSF (Fig. 2.2). In this way, the LSF can be sampled with an effective sampling frequency high enough to avoid aliasing, and hence the presampling MTF is obtained. There are no restrictions on the presampling MTF as with the two formerly described methods, since the effective sampling frequency of the method can be adjusted by changing the angle of the slit relative to the sampling coordinates. The solution of tilting the object has also been adopted and adapted to the edge and SWRF methods, and several publications cover the theory of the methods and details of their implementation for digital radiographic systems [33,38,71,73,84,85].

All experimental determinations of the one-dimensional presampling MTF in the present work (Papers II-V) were performed using the tilted slit method. A slit was made by placing two aluminium foils of thickness 10 μm between two pieces of carefully polished tungsten of thickness 2 mm, width 9 mm and length 30 mm, attached to a holder of steel (Fig. 2.3). The two foils were placed at the ends of the pieces of tungsten in such a way that, after tightly screwing the two pieces together, a slit was formed by the air gap between the two pieces of tungsten. By inspection with a microscope, the slit was found to be 11±1 μm wide. The construction was mounted on a bottom plate, which made it possible to rotate the slit in two dimensions for alignment with the X-ray beam and to obtain any angle between the slit and the sampling coordinates. Images were collected at high mAs values. After linearization, a finely sampled LSF was obtained with the tilted slit method described by Fujita *et al.* [4]. A small background caused by transmission through the jaws of the slit was subtracted from each LSF. The background level was usually obtained from the area between 5 and 10 mm from the slit. Furthermore, exponential extrapolation below the 1% level of the LSF was employed to handle the noisy tails, except in the study described in Paper II where the 2% level was used due to an asymmetrical LSF in the subscan direction of the CR system being investigated. In Fig. 2.4, the presampling MTFs of a number of systems evaluated in the present work are presented.

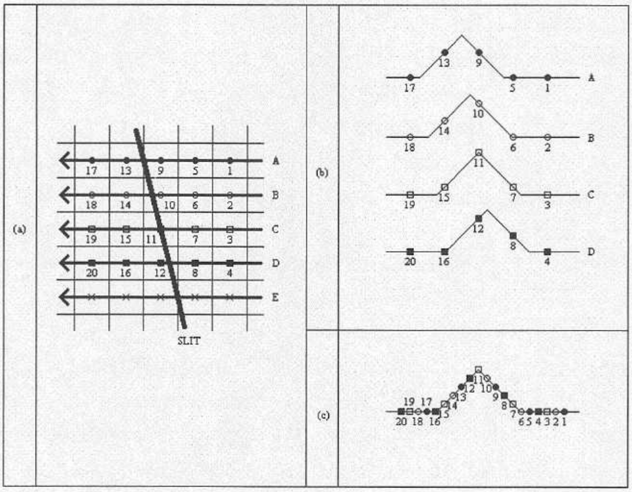

Figure 2.2. Schematic drawing showing the generation of a finely sampled LSF (c) from the LSFs (b) from different alignments of the slit relative to the sampling coordinates (a). (Slightly modified from Fujita *et al.* [4].)

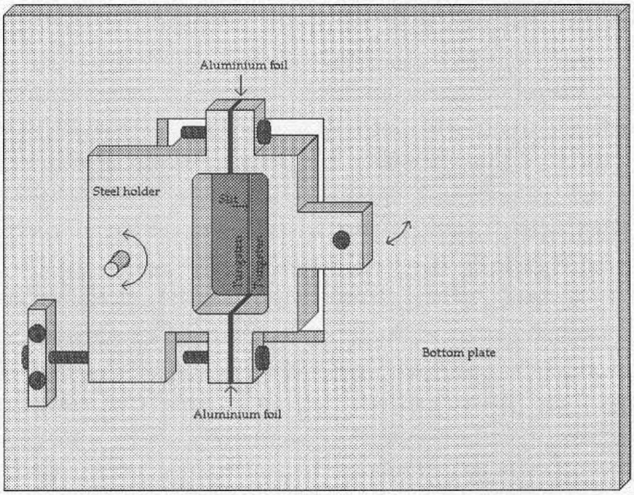

Figure 2.3. Drawing of the slit used for one-dimensional MTF determinations. The slit is rotateable in two dimensions for alignment with the X-ray beam and to obtain any angle between the slit and the sampling coordinates.

Using exponential extrapolation of the tails is a common method to handle noisy data, and the 1% level is usually used [4,33,38,71]. However, using a different extrapolation level [40,86] or smoothing the tails [39,87] of the LSF – obtained directly using the slit method or via the ESF – has also been employed. An alternative method is to fit an analytical function to the LSF and use this function in the subsequent calculation of the MTF [88]. It should be noted that when extrapolation of the LSF is used, there is an evident risk that the effects of low-intensity information at the ends of the tails, such as glare, will be neglected. This low-intensity information may result in what is called a low-frequency drop, meaning that the MTF drops immediately above zero frequency. Extrapolation of the tails tends to remove this drop and the resulting MTF decays smoothly from the zero-frequency value of unity. When Fujita *et al.* [4] presented the tilted slit method with extrapolation for determining the one-dimensional presampling MTF, they also presented a determination of the glare fraction to compensate for the removal of the low-frequency drop. However, this component is often neglected in the determination of the presampling MTF and the DQE in such a way that the LSF is extrapolated without separate determination of the glare fraction [33,36-38,40,71]. It should therefore be borne in mind that many estimates of the presampling MTF and the DQE may be overestimated. This is also the case in this work. Another objection against the slit method is that it probes the system simultaneously at very high and very low intensities, and that this leads to problems if the system is not considered linear in the intensity range under consideration [84].

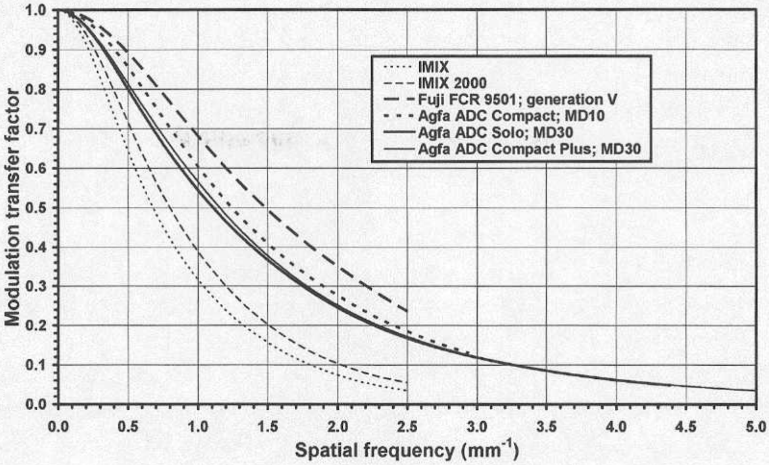

Figure 2.4. Presampling MTFs of six systems evaluated in the present work presented up to the Nyquist frequency. The data presented are the average of one-dimensional determinations in orthogonal directions centrally using the tilted slit method (IMIX: only vertical direction). Data on the systems (system, pixel size, paper where evaluated): IMIX, 0.200 mm, Papers IV+V; IMIX 2000, 0.200 mm, Papers IV+V; Fuji FCR 9501 with generation V image plates, 0.200 mm, Paper V; Agfa ADC Compact with MD10 image plates, 0.170 mm, Paper V; Agfa ADC Solo with MD30 image plates, 0.114 mm, Paper II; Agfa ADC Compact Plus with MD30 image plates, 0.100 mm, Paper III).

If data belonging to the crossing of one pixel row by the slit are used for each finely sampled LSF, the angle used to position the slit slightly tilted relative to the sampling coordinates is a trade-off between high sampling frequency and low statistical uncertainty. With a small angle, the tilted slit method provides a means of sampling at a very high frequency, since the sampling frequency is proportional to the reciprocal of the tangent of the angle. However, since the frequencies of interest often range from zero to the true Nyquist frequency of the system, it is sufficient to sample at a frequency allowing correct determination of frequencies in this range. This is done by ensuring that the sampling frequency used is high enough to exclude aliasing, and also high enough to ensure that the resampling of the finely sampled LSF does not influence the result. Therefore, one may choose a relatively large angle since the use of such an angle results in a larger number of MTFs that can be averaged, thereby resulting in lower uncertainty. By choosing an angle that ensures a sampling distance that is at least five times smaller than the true sampling distance of the system, the two requirements are usually fulfilled. With a slit of length 30 mm, up to 30 realizations of the presampling MTF can be determined on a system with 200 μm pixels with a single exposure. Since each exposure causes a heavy load on the tube due to the small dimensions of the slit, a reduction in the number of exposures is desirable. Finally, the fact that the presampling MTF is determined in the direction orthogonal to the slit must be addressed. If the intention is to measure the presampling MTF along a coordinate axis of the system, a smaller angle must be used to ensure that the presampling MTF is determined close to the axis. In the present work, angles ranging from approximately 2° to 5° were used, resulting in approximately 5-10 realizations of each presampling MTF for systems with a sampling distance of 0.2 mm, and approximately 10-20 for those with a sampling distance of 0.1 mm. (Data from the ends of the slit were not used, since the slit cannot be regarded as a line source at distances from the ends comparable to the dimensions of the LSF.)

2.4 Simulating the MTFs of digital radiographic systems (Paper I)

The aim of Paper I was mainly to theoretically investigate the effects on the MTF of the design of a digital radiographic detector. A computer program – *MTF Simulator** – was therefore developed in IDL (Research Systems, Inc., Boulder, Colorado, USA) (Fig. 2.5). The program simulates a digital radiographic system using three parameters: sampling distance, sampling aperture (assumed to be continuous, quadratic and centred on the sampling point) and the spread of the signal in the detector due to the interaction processes of the incoming photons, approximated by two Gaussians. (The full width at half maximum – FWHM – and the relative weight of each Gaussian is given as input.) Given these data as input, the program gives the presampling MTF, the sampling aperture MTF (MTF_S), and the two extreme cases of the MTF_d – the maximum MTF (MTF_{max}) and the minimum MTF (MTF_{min}). The program does not assume rotational symmetry, but has the limitation that the MTFs are only determined along the coordinate axes. The simulations are performed in the spatial domain, and are therefore not explicitly based on Eq. (2.15). The presampling MTF is obtained from the 'finely sampled' LSF that is the result of averaging the LSF from the Gaussians in the sampling aperture. This LSF is then sampled at a large number of phases ranging from the central alignment – the sampling points are positioned in such a way that the input signal is centred on a sampling point – to the shifted alignment – the input signal is centred between two sampling points. The different MTF_ds corresponding to the different sampled LSFs are calculated and the MTF_{max} and MTF_{min} are defined as the MTF_ds that result in the largest and smallest values when integrated, respectively. The program also simulates a measurement of the presampling MTF with a slit, where the slit width can be chosen arbitrarily. This is achieved by distributing finely sampled LSFs over a distance corresponding to the width of the slit and then at each location adding the contributions from all finely sampled LSFs.

---

*MTF Simulator can be obtained at http://www.radfys.gu.se/downloads or directly from the author.

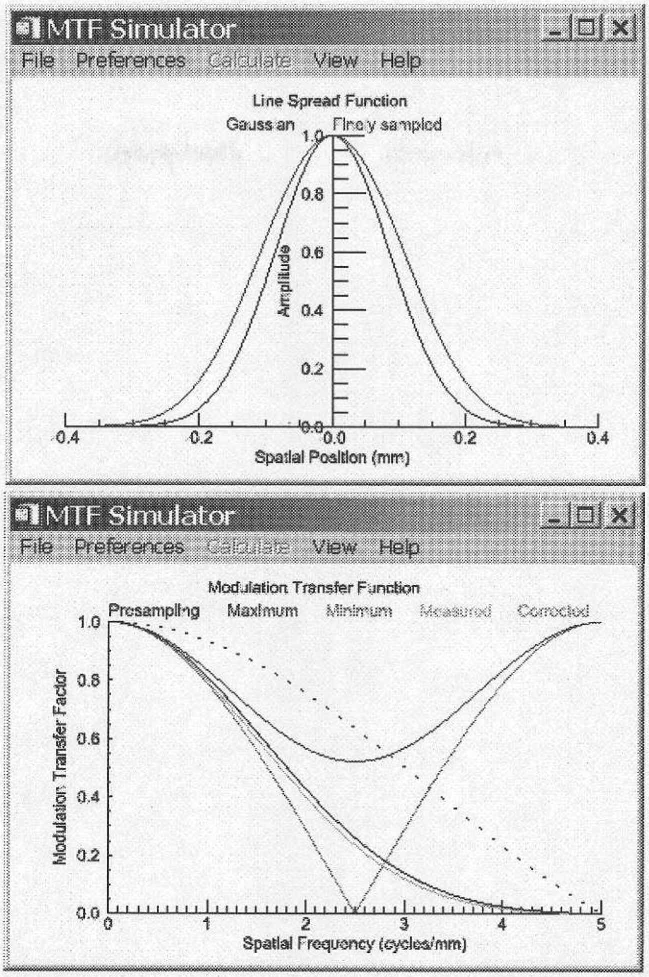
MTF Simulator
File Preferences Calculate View Help
Line Spread Function
Gaussian
Finely sampled
Amplitude
1.0
0.8
0.6
0.4
0.2
0.0
-0.4
-0.2
0.0
0.2
0.4
Spatial Position (mm)
MTF Simulator
File Preferences Calculate View Help
Modulation Transfer Function
Presampling
Maximum
Minimum
Measured
Corrected
Modulation Transfer Factor
1.0
0.8
0.6
0.4
0.2
0.0
0
1
2
3
4
5
Spatial Frequency (cycles/mm)

Figure 2.5. Screenshots of MTF Simulator. A detector with a sampling distance of 0.2 mm, sampling aperture 0.2×0.2 mm^2 (fill factor 100%) and FWHMs of the Gaussians – describing the spread of signal due to the interaction processes of the photons – of 0.2 mm is simulated. A measurement of the presampling MTF with the slit method is also simulated with a slit width of 0.1 mm.

The program was used to study the influence of the three parameters mentioned above on the resulting MTFs. It was found that the central MTF does not necessarily result in the maximum MTF, which is sometimes taken for granted [65,89]. For a specific configuration of a detector of sampling distance 0.2 mm, sampling aperture 0.4×0.4 mm^2 and FWHMs of the Gaussians of 0.2 mm, it was found that the central alignment actually resulted in $\mathrm{MTF}_{\mathrm{min}}$. Such a configuration, although not common, can be obtained by filtering the signal prior to sampling. It was also shown, not surprisingly, that the amount of aliasing increases when the width of the LSF from the Gaussians decreases, and that the same result is obtained when the sampling aperture is decreased, if the system is undersampled. This is of course due to the fact that a narrower finely sampled LSF, which is the result in both cases, constitutes a higher proportion of frequencies above the Nyquist frequency, which contaminate the frequencies below the Nyquist frequency at sampling. However, it was shown for a particular system that if the sampling distance was decreased as the sampling aperture was decreased so that the fill factor was kept constant, this resulted in less aliasing. (The fill factor is often used to describe the proportion of a pixel that is sensitive to radiation and was generalized to the ratio of the sampling aperture to the squared sampling distance in Paper I.)

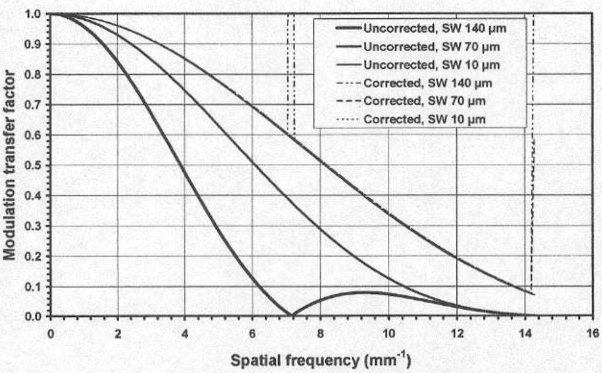

Figure 2.6. Simulations of measured presampling MTFs, before and after correction for the slit width, of a system with a FWHM of the Gaussian of 33 µm, a sampling distance of 70 µm, and a sampling aperture of 60x60 µm². Slit widths (SW) used are 10, 70, and 140 µm. (Note: several overlapping curves.) (Redrawn from Paper I.)

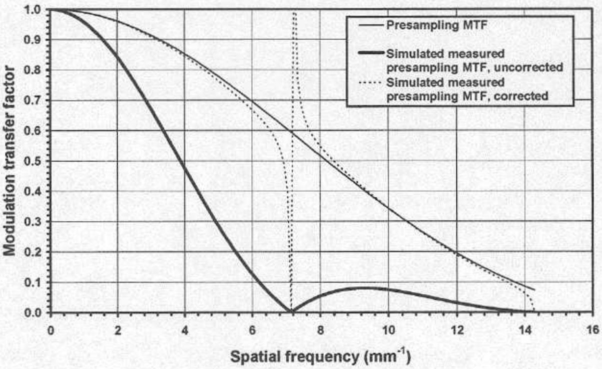

Figure 2.7. Different MTFs of a system with a FWHM of the Gaussian of 33 µm, a sampling distance of 70 µm, and a sampling aperture of 60x60 µm². Slit widths used: 140 µm for measurement, 139 µm for correction. (Redrawn from Paper I.)

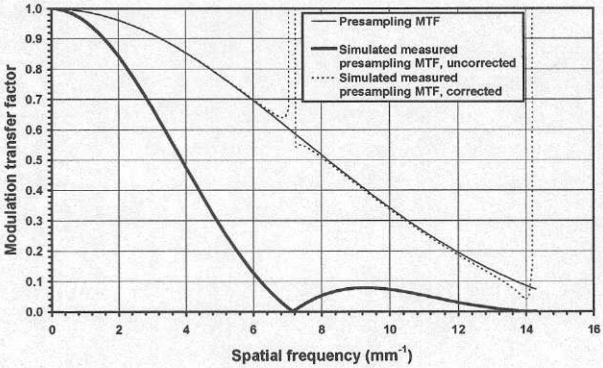

Figure 2.8. Different MTFs of a system with a FWHM of the Gaussian of 33 µm, a sampling distance of 70 µm, and a sampling aperture of 60x60 µm². Slit width used: 140 µm. Noise added to the finely sampled LSF. (Redrawn from Paper I.)

Regarding the simulations of measurements of the presampling MTF with the slit method, the presampling MTFs obtained with, as well as without, correction for the slit width are obtained with the program. It is sometimes stated that the size of the slit used when measuring the LSF must be small compared with the LSF or the pixel size. Yu *et al.* [90] for example, used the edge method instead of the slit method when determining the MTF of phosphor screens with a CCD camera with a pixel size of 20 μm, with the motivation that a slit with a width <<20 μm was not available. However, in Paper I it was shown that there are no theoretical restrictions on the size of the slit as long as the dimensions of the slit are known with sufficient accuracy (Fig. 2.6). In the non-ideal case with noise in the measurements, penetration of radiation through the edges of the slit and where the slit width is not exactly known, a substantial error will be introduced if the slit is large compared with the pixel size. However, when using an extremely large slit, with a width of twice the sampling distance, the error arising from using the 'wrong' slit width for the correction can be easily identified (Fig. 2.7). Also, the error due to noise was not very large, and the major part of the MTF was unaffected (Fig. 2.8). These results indicate that measurements of the LSF, or the PSF, can be based on objects with finite extensions.

2.5 Determining the two-dimensional presampling MTF (Paper II)

As has already been mentioned, measurements of the presampling MTF have usually been performed in a one-dimensional manner. However, for digital radiographic systems there is a lack of rotational symmetry, due to both non-circular sampling apertures (leading to a rotationally asymmetric presampling MTF), and varying sampling frequencies in different directions (leading to different amounts of aliasing in different directions). The aim of the work described in Paper II was therefore to develop a method for determining the two-dimensional presampling MTF from the PSF of a digital radiographic system. Two problems had to be solved. 1) Already with the slit method, the penetration through the measurement device is very small; leading to exposure settings of hundreds of mAs (with a typical slit width of 10 μm). A hole with this diameter would result in virtually no penetration. 2) To avoid aliasing, the PSF has to be oversampled in a manner similar to that in the tilted slit method, where the slit is positioned at a slight angle relative to the sampling coordinates, and data from several rows are used to construct a finely sampled LSF (Fig. 2.2).

1) The first problem was addressed with a result from Paper I in mind – that there really are no theoretical restrictions on the slit width if the dimensions are known with sufficient accuracy. In fact, for a linear stationary system, Eq. (2.9) can be transformed into:

$$MTF(u,v) = \frac{|G(u,v)|}{|F(u,v)|} \qquad (2.17)$$

if the right-hand side of Eq. (2.17) is normalized to unity at zero frequency. Therefore, as long as the Fourier transform of the input signal (the imaged object), F, is known, the MTF can be obtained from the Fourier transform of the output signal (the image), G, and virtually any object can be used to determine the MTF. (In theory, restrictions apply only due to zero values of F. In reality, however, noise will lead to uncertainties whenever F is small, as will uncertainties in F.) In order to be able to make use of the simplifications resulting from rotational symmetry of the input signal, a disk-shaped hole with rather large dimensions was considered a suitable object. The response of the system to such a hole, *i.e.* the convolution of the PSF and the ideally disk-shaped projection of the hole, was termed the *disk spread function* (DSF).

2) As mentioned previously, a digital radiographic system is, in most cases, not stationary, and the DSF has therefore to be finely sampled to avoid artefacts due to aliasing. This second problem can be solved in two different ways: i) by repeated exposure of a single hole where the hole is shifted relative to the sampling coordinates between each exposure in order to finely sample the DSF, or ii) by using several holes positioned at different phases and constructing a finely sampled DSF from the DSFs obtained from each hole, which is conceptually similar to the tilted slit method in the one-dimensional case [4,33]. The latter solution was used and a so-called *aperture mask* was constructed consisting of one hundred holes drilled in a 10×10 matrix in a 2 mm thick alloy of lead (94%) and antimony to achieve both the attenuating properties of lead as well as sufficient rigidity to ensure that the aperture mask would not easily be deformed (Fig. 2.9). The holes had a diameter of 0.48 mm and were separated by a distance of 5.04 mm, resulting in holes over an area of 46×46 mm^2.

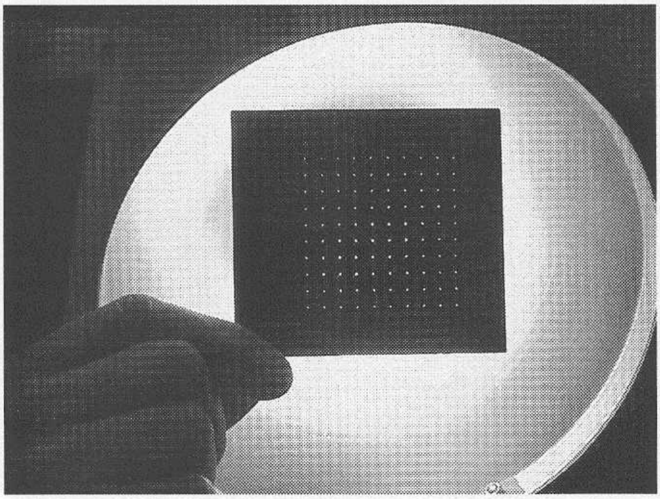

Figure 2.9. The aperture mask used for the study described in Paper II.

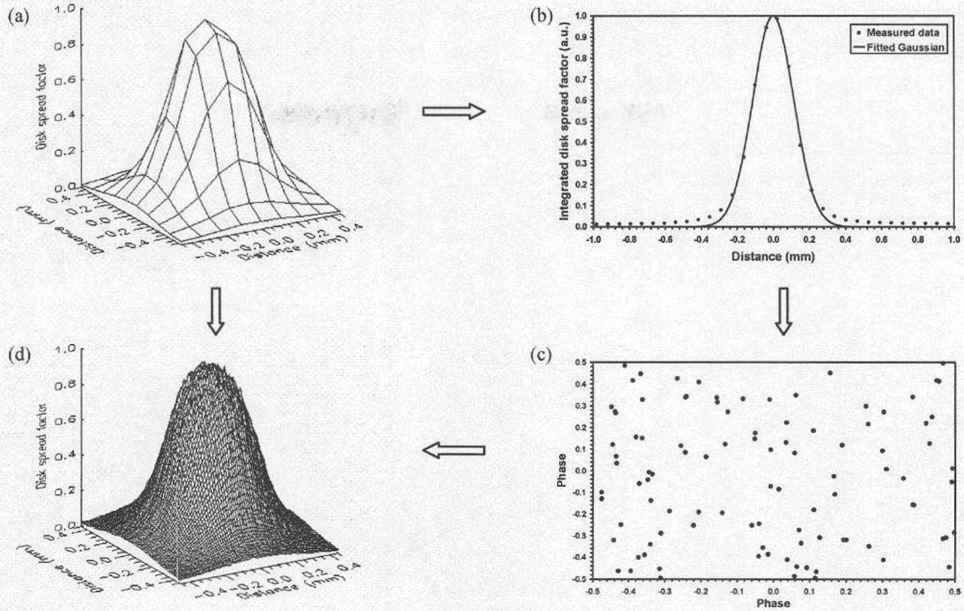

Figure 2.10. Determination of a finely sampled DSF. Each DSF is localized (a) and integrated in orthogonal directions. A Gaussian is fitted to each integrated DSF (b) and the phase of the hole relative to the sampling coordinates is obtained (one of the two integrated DSFs is shown). The phase information from all 100 holes (c) is used together with the 100 DSFs to construct a finely sampled DSF (d). (Redrawn from Paper II.)

The aperture mask method was tested on the Agfa ADC Solo CR system (Agfa-Gevaert, Mortsel, Belgium) using MD30 image plates read in high-resolution mode. The aperture mask was placed on the image plate, which was positioned on a stand in order to enable the centre of the mask to be positioned orthogonal to the X-ray beam axis. Images of the aperture mask were collected at a beam quality given by a tube voltage of 70 kV_P and a filtration (total filtration + added thickness of Al) equivalent of 19 mm of Al, with a distance of 210 cm between the focal spot and the detector. The images were transferred to a PC and linearized through the relationship between pixel value and entrance air kerma free in air (K_{air}), determined by the collection of flat-field images. The method used for constructing a finely sampled DSF from an aperture mask image is presented graphically in Fig. 2.10. Each DSF (constituting a region of interest – ROI – of size approximately 5×5 mm^2) was normalized to unity volume and integrated in the x- and y-directions. The integrated values in each direction were then fitted to a Gaussian, whereupon the phase was obtained as the distance between the position corresponding to the maximum value of the Gaussian and the position corresponding to the maximum value of the DSF, divided by the sampling distance. In this way, phases ranging from –0.5 to 0.5 were obtained in both directions. Using the phase information, a finely sampled DSF was obtained from all 100 DSFs. This DSF was then resampled by linear interpolation to obtain a finely sampled DSF with equidistant sampling (resampled DSF) and exponentially extrapolated in a radial manner below the 1% level. The sampling distance of the resampled DSF was 0.0114 mm in each direction, corresponding to one tenth of the sampling distance of the system.

The two-dimensional presampling MTF was obtained by Fourier transformation of the resampled DSF after correction for the finite hole size according to Eq. (2.17), where $|F(u,v)|$ is given by the modulus of the Fourier transform of a circular disk [91]:

$$|F(u,v)| = \begin{cases} a\pi r^2, & if(u,v)=(0,0) \\ \left|\dfrac{arJ_1\left(2\pi r\cdot\sqrt{u^2+v^2}\right)}{\sqrt{u^2+v^2}}\right|, & if(u,v)\neq(0,0). \end{cases} \tag{2.18}$$

In. Eq. (2.18), J_1 is the first-order Bessel function of the first kind, r is the radius of the disk, and a is the intensity of the disk. The appropriate hole radius was determined in a semi-empirical manner by examining the effects of the correction (Fig. 2.11). For comparison with a more established method, the one-dimensional presampling MTF was determined using the tilted slit method.

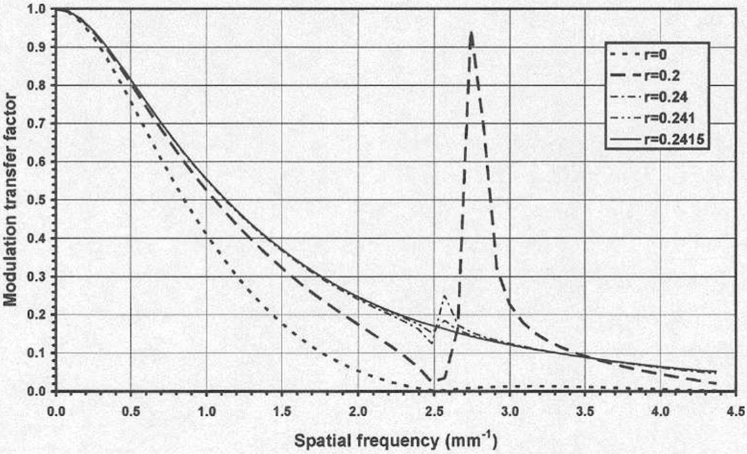

Figure 2.11. The shape of a cut through the origin of the two-dimensional presampling MTF when using different disk radii to correct for the hole size. Radii in mm. r=0 corresponds to no correction. (Redrawn from Paper II.)

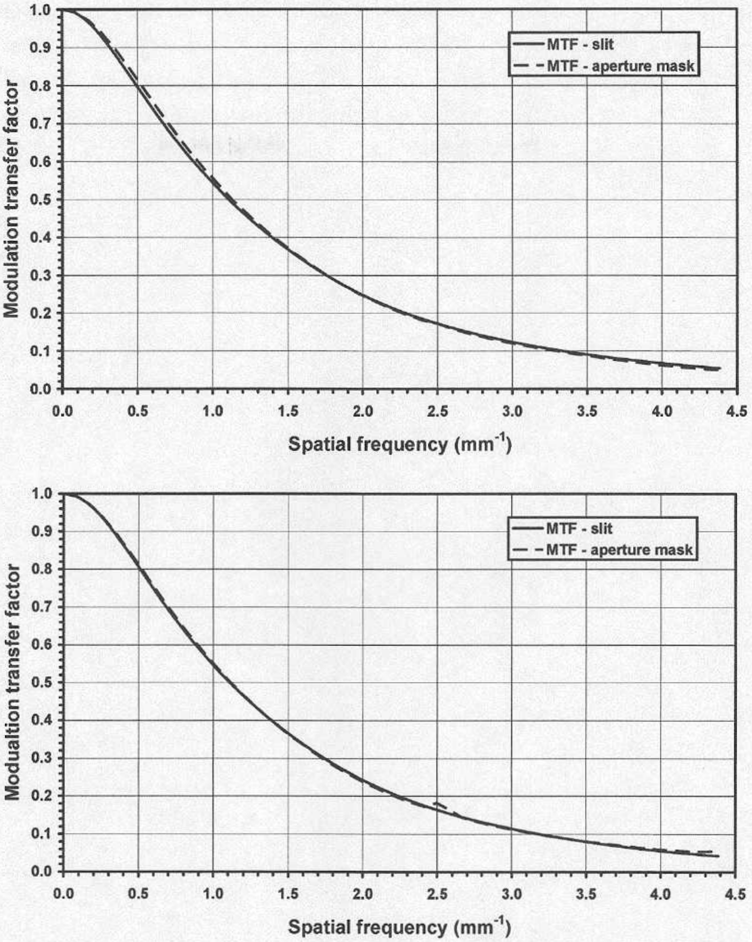

Figure 2.12. One-dimensional presampling MTFs of the Agfa ADC Solo with image plates of type MD30, in directions close to the subscan (top) and scan (bottom) directions, obtained with the tilted slit and aperture mask methods. Presampling MTFs from the aperture mask method represent cuts through the origin of the two-dimensional MTF. (Redrawn from Paper II.)

The agreement between the aperture mask method and the tilted slit method in determining the one-dimensional presampling MTF – obtained as a cut through the origin of the two-dimensional MTF with the aperture mask method – was very good when the disk radius used for the correction for the hole size was adjusted independently for each one-dimensional presampling MTF (Fig. 2.12). However, there was a small variation in the optimum disk radius in different directions (Paper II, Table 1), which led to large errors at frequencies for which the correction for the hole size was large when a single disk radius was used to determine the complete two-dimensional presampling MTF. This error, caused by the use of a non-optimal disk radius, was larger than 5% already at a frequency of 2.3 mm^{-1} due to the large hole size (diameter 0.48 mm) (Fig. 2.13). Nonetheless, the study showed that the concept of the aperture mask method could be used to determine the two-dimensional presampling MTF of a digital radiographic system, but that an aperture mask with smaller holes was needed to achieve sufficiently high reliability for all frequencies up to the Nyquist frequency.

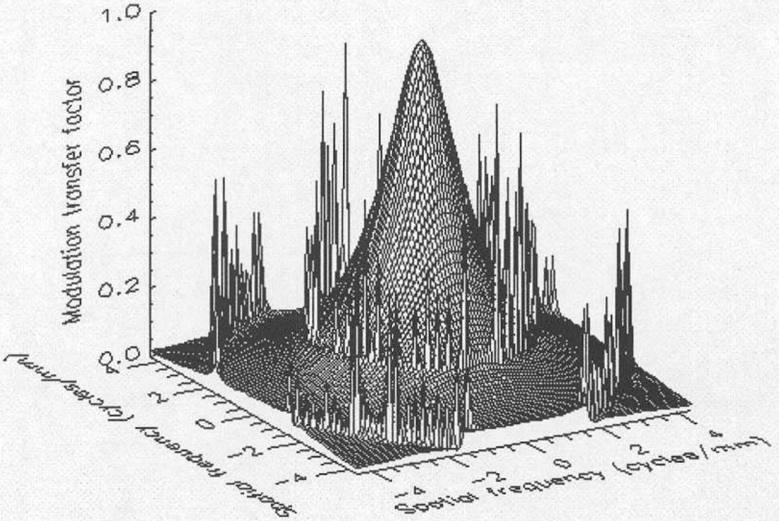

Figure 2.13. Two-dimensional presampling MTF of the Agfa ADC Solo using image plates of type MD30 read in high-resolution mode, obtained with the aperture mask method. The artefacts at approximately 2.5 mm^{-1} and 4.6 mm^{-1} are due to the correction for the sizes of the holes in the aperture mask. The x-axis corresponds to the subscan direction.

2.6 Noise power spectrum

2.6.1 The NPS of an analogue system

In Sections 2.1 and 2.3 the imaging system was treated mainly as a deterministic system. However, noise processes are present in any imaging system. These can also be described in detail in the frequency domain, in a way similar to that of the signal transfer, through the use of the noise power spectrum (NPS) or – as it is sometimes called – the Wiener spectrum. The NPS of a stationary ergodic random process D(x,y) – ergodic meaning that expected values can be determined equivalently from ensemble averages or spatial averages [29] – is defined by [63]:

$$NPS(u,v) = \lim_{\substack{X\to\infty \\ Y\to\infty}} \left\langle \frac{1}{2X}\frac{1}{2Y}\left|\int_{-X}^{X}\int_{-Y}^{Y}\Delta D(x,y)e^{-2\pi i(ux+vy)}dxdy\right|^{2}\right\rangle, \qquad (2.19)$$

where the angled brackets denote the ensemble average. The NPS describes the frequency components of the noise and can be interpreted both as the pixel variance spread over spatial frequencies and the uncertainty in the measurement of a particular frequency [66]. Several publications cover the topic of the NPS in imaging [29,63,66].

2.6.2 The NPS of a digital radiographic system

In order to use Fourier-based descriptions of the noise properties of a system, the system has in theory to obey the rules of stationarity and ergodicity [29]. Although digital radiographic systems are very seldom stationary or ergodic, the NPS concept is widely used for these systems. The matter of stationarity can be addressed by arguing that although a system is non-stationary, no problems arise due to phase dependence since the NPS is defined as an ensemble average which includes contributions from all possible phases of the noise [66]. Regarding ergodicity, although digital imaging systems are seldom truly ergodic, they can often be approximated as such [29]. The digital NPS (NPS_d) – the NPS of a digital system – has therefore been expressed in a way similar to the digital OTF and the digital MTF [92]:

$$NPS_d(u,v) = NPS_A(u,v)\left|OTF_S(u,v)\right|^2 \otimes \sum_{m=-\infty}^{\infty}\sum_{n=-\infty}^{\infty}\delta\left(u-\frac{m}{\Delta x}, v-\frac{n}{\Delta y}\right), \tag{2.20}$$

where NPS_A is the analogue input NPS. The product of NPS_A and $|OTF_S|^2$ has been referred to as the presampling NPS, analogous to the presampling MTF and the presampling OTF [65].

When comparing with Eq. (2.15), it is evident that there is no phase dependency of NPS_d. The 'd' is therefore most often omitted, and the term NPS is used also for digital systems. Furthermore, NPS_d is the only NPS available, since the presampling NPS cannot be measured [65].

2.6.3 Determining the NPS of a digital radiographic system

One way of expressing the NPS of a digital imaging system, which can be used for determining the MTF of a digital radiographic system, is [66]:

$$NPS(u,v) = N_x N_y \Delta_x \Delta_y \left\langle \left| FT\{\Delta I(x,y)\} \right|^2 \right\rangle, \tag{2.21}$$

where ΔI is the deviation from the mean of a noise image (flat-field image) and N_x and N_y are the number of pixels and Δ_x and Δ_y the pixel sizes in the x- and y-directions, respectively. Equation (2.21) can also be found with the product $N_x N_y$ in the denominator instead of in the numerator [33]. Different FFTs may use different scaling, as was previously mentioned, and it is therefore important to check the calculations by making sure that the integral of the two-dimensional NPS is equal to the variance of the pixel values in the image [33]. If this is not the case, the obtained result must be scaled in order for the relationship to hold. Usually, the scaling factor can be based on the product N_xN_y.

The ensemble average is usually replaced by a spatial average in that the image is divided into several ROIs. For each ROI, after subtraction of the mean of the ROI, the square of the modulus of the Fourier transform of the pixel values is calculated. The results from all ROIs are then averaged. Using spatial averages instead of ensemble averages in theory demands that the system is ergodic which – as has already been mentioned – digital radiographic systems very seldom are, but often can be approximated as such.

A problem associated with measuring the NPS is that limited amounts of data are available. This leads to uncertainties in the estimations, and a compromise between frequency resolution and precision therefore has to be made. The larger the ROIs, the better the frequency resolution, but, at the same time, the uncertainty in the determination of a specific frequency increases. The decision about when the best compromise is reached for a limited amount of data is somewhat subjective [33], but recommendations exist [66]. One way of increasing the precision without losing frequency resolution is of course to use several images and divide each image into several ROIs. If this is done, it is important to shift the position of the ROIs between each image so that no two ROIs are positioned over the same area [66]. If this is not done, the structured noise of the imaging detector will be underestimated.

In practice, determinations of the NPS will include an effect from the finite window used for the measurement. When the Fourier transform is applied to the ROIs directly, as described above, this leads to a convolution of the true measurable NPS with a squared sinc function ('spectral leakage') [65]. The term 'windowing' is used to describe the method of altering the noise data in each ROI so that the effect of the finite window is reduced. Several windowing functions exist [93], but there is no consensus regarding the use of any one specific windowing function. Often, windowing is therefore not used.

In the present work, different approaches for determining the NPS were used. Windowing was, however, never used. In two of the studies (Papers IV and V), a single flat-field image was used at each K_{air} level examined. In the latter (Paper V), the noise image was divided into ROIs of 128×128 pixels, and the Fourier transforms of each of these were calculated and averaged. In the former (Paper IV), a single ROI of 1024×1024 pixels was used in each image, and binning in the frequency domain was employed, meaning that the averaging was performed in the frequency domain rather than in the spatial domain. The reasons for this were to reduce the spectral leakage and the fact that the systems investigated showed clear signs of nonergodicity (Paper IV, Fig. 2). However, the conventional method of dividing the image into ROIs of 128×128 pixels was also tested and the difference in the results was minor.

In another study (Paper III), 64 flat-field images were used at a single K_{air} level. Each image was divided into ROIs of 256×256 pixels in size which were then Fourier transformed and averaged. The ROIs were shifted $256/\sqrt{64}=32$ pixels in the x- or y-direction between each image. The larger ROI size was used since the smaller pixel size of the system evaluated in the study led to too much spectral leakage at low frequencies when ROIs of 128×128 pixels were used.

The reason for the difference in the number of images used at each K_{air} level was that in the study described in Paper III the two-dimensional NPS was used for further calculations, whereas it was mainly used to obtain a one-dimensional NPS in the two other studies (Papers IV and V). Determination of the one-dimensional NPS requires less image data to obtain a certain level of precision for a specific frequency since the two-dimensional NPS data can be averaged to obtain the one-dimensional NPS.

2.6.4 Obtaining a one-dimensional NPS

It may be useful to study the two-dimensional NPS, since it often reflect artefacts of the system. However, if the NPS is used together with the one-dimensional MTF in calculating the NEQ or the DQE (see Section 2.7), a one-dimensional representation of the NPS must be used. This can be obtained in two ways for digital imaging systems: either the one-dimensional NPS can be determined directly or a one-dimensional description of the NPS can be obtained from the two-dimensional NPS.

1) Determining the one-dimensional NPS directly is usually performed with the synthesized scanning slit method [10,30,31,36,37,40,43,92,94,95]. With this method, the noise image is divided into several ROIs. In each ROI, the data is averaged in one direction. The resulting 'slit trace' represents one-dimensional noise data and can be Fourier transformed to obtain the one-dimensional NPS.

2) For the determination of the one-dimensional NPS based on the two-dimensional NPS, data along a slice of the two-dimensional NPS, in theory, correspond to the one-dimensional NPS in that direction [29]. However, to decrease the statistical noise, averaging of the two-dimensional NPS is usually employed to obtain a one-dimensional NPS. Different alternatives exist, but the two most common ones are to use radial averaging [44,93] or axial averaging [33,38,41,96] of the two-dimensional NPS (Fig. 2.14). (Since the presampling MTF is usually determined close to the coordinate axes, so is the one-dimensional NPS.) In the former method, data within a sector of the two-dimensional NPS are averaged and in the latter, data within a few lines on each side of the axis of the two-dimensional NPS are used. With the latter method,

data on the axis itself are usually excluded, particularly in CR, since they are usually not representative of the noise behaviour, due to *e.g.* readout noise. In both methods, the frequency value for the one-dimensional NPS was computed as $\sqrt{(u^2+v^2)}$ for each frequency value (u,v) in the used part of the two-dimensional NPS. The radial averaging usually results in a lower uncertainty since a larger part of the two-dimensional NPS is used. However, if the rotational symmetry is low, the use of a radially averaged one-dimensional NPS together with the presampling MTF may lead to an erroneous determination of the DQE. On the other hand, if the one-dimensional NPS is used only to describe the noise properties of the system, radial averaging results in a more valid result than axial averaging.

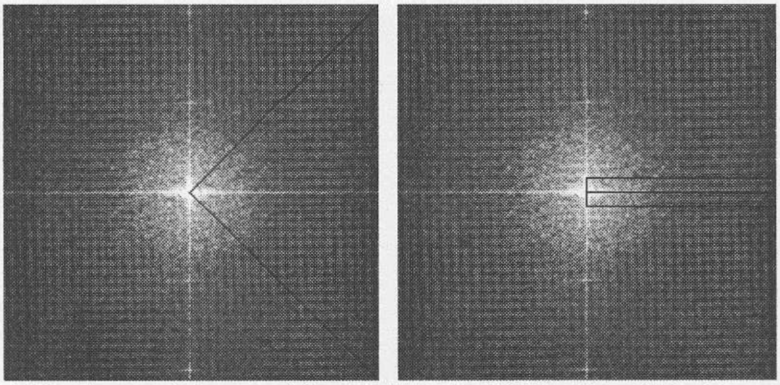

Figure 2.14. Visualization of the part of the two-dimensional NPS within which data were used to obtain a one-dimensional NPS in the horizontal direction in the present work, using radial averaging (left) and axial averaging (right).

In the present work, both axial and radial averaging were used. In the work presented in Paper V, the one-dimensional NPS was used only to determine the DQE, and axial averaging of four lines on each side of the axis was used. In the work described in Paper IV, radial averaging was used since the one-dimensional NPS was studied, although this NPS was also used to determine the DQE. In Paper III, both methods were used to illustrate the difference in the obtained DQE.

2.6.5 Normalized NPS

In a similar way as the relative standard deviation is used to describe the relative uncertainty in the determination of a random process by dividing the standard deviation with the mean, a normalized NPS (NNPS) can be used to describe the relative uncertainty in the determination of the frequency components of a random process. Normalization is achieved by dividing the NPS by the square of the 'large area signal' [66]:

$$NNPS(u,v) = \frac{NPS(u,v)}{(large\ area\ signal)^2}. \qquad (2.22)$$

'Large area signal' is the term commonly used for the average of the noise process (the average pixel value in a flat-field image). The reason for squaring it in the denominator is that the NPS is a measure of the variance of the spatial frequencies, not the standard deviation. The NNPS is therefore the square of the relative standard deviation or the relative variance of the frequency components of the noise.

The reasons for using the NNPS are two. First of all, normalization results in a measure that is unaffected by amplification, meaning that the NNPS can be used to compare the noise on different scales. Secondly, the use of the NNPS may improve the precision of the noise-power measurement. The 'flat field' from an X-ray tube is not flat, due to the heel effect and the divergence of the field, for example. This leads to variation in the exposure over the measurement area. If spatial averages instead of ensemble averages are used, the averaging of calculations of the NNPS of each ROI tends to cancel some of the variations in noise power resulting from regional variations in X-ray exposure [66]. The NNPS was used for all NPS determinations in the present work.

2.7 Detective quantum efficiency: expansion of the concept

In Section 2.2, the DQE was introduced as a measure that describes the signal-to-noise transfer of a photon-counting detector compared to that of an ideal detector. In this section, the DQE concept will be expanded into a measure that completely describes the imaging properties of a digital radiographic system in the sense that it describes the efficiency of the system to extract information from a radiation beam [97]. However, there are limitations to its validity as a measure of the clinical performance of a system [97], and these will be explored in Chapter 3.

2.7.1 Frequency dependency

Although being a fundamental property of a detector, the DQE expressed as in Eq. (2.10) does not give enough information about an imaging system to be useful, since it does not take the resolution properties of the detector into account. This problem can be solved by expressing the DQE as a function of spatial frequency. As such, it can describe the efficiency of the imaging detector completely, since, for any given spatial frequency it would state the efficiency of the system in detecting that frequency compared with that of the ideal detector, which is ideal both in terms of detection and localization of the incoming quanta.

It can be shown that the DQE concept can be expanded to an explicit function of spatial frequency using the MTF and the NPS for a radiographic system [63,98]. A common expression of the frequency-dependent DQE for a linear or linearized detector is [66]:

$$DQE(u,v) = \frac{MTF^2(u,v)}{NNPS(u,v)SNR_{in}^2} \tag{2.23}$$

The introduction of the MTF and the NPS can intuitively be understood as the frequency-dependent signal and noise at the output. The reason for the noise being normalized (the NNPS is used) is that the MTF is already normalized by definition. SNR_{in}^2 may also be expressed as a function of spatial frequency, although the assumption of white noise in the input signal leads to one and the same value of $SNR_{in}^2(u,v)$ for all frequencies, identical to the scalar SNR_{in}^2. The zero-frequency value of DQE(u,v) is also identical to the scalar DQE described in Section 2.2 [66].

2.7.2 NEQ

The ratio of the square of MTF and the NNPS is the frequency-dependent NEQ of an image [66]:

$$NEQ(u,v) = \frac{MTF^2(u,v)}{NNPS(u,v)}. \tag{2.24}$$

The NEQ is a measure of the square of the frequency-dependent SNR in the image. The NEQ for a real system can therefore be interpreted as the number of quanta per unit area that an ideal system would need to image a certain frequency with the same SNR as the real system. While the DQE is a quantity describing the quality of *the imaging system*, the NEQ describes the quality of *the image*. When model (mathematical) observers are used to determine the SNR of a specific discriminating task, the NEQ is a fundamental property of the image [99].

2.7.3 The ideal detector and the problem of determining SNR_{in}

Due to the Poisson distribution of the incoming quanta, early descriptions of DQE used the number of quanta as SNR_{in}^2 [63,98]. However, since radiographic detectors usually integrate the energy deposited by the detected photons rather than count their number, and since the radiation is polychromatic, SNR_{in}^2 is usually calculated using energy weighting of the quanta, where each quantum is weighted proportionally to its energy. The expression for SNR_{in}^2 is then given by [30]:

$$SNR_{in}^2 = \frac{\left(\int_0^{E_{\max}} q(E)E\,dE\right)^2}{\int_0^{E_{\max}} q(E)E^2\,dE}, \tag{2.25}$$

where q(E) is the number of quanta per unit energy with energy E. Using Eq. (2.25) to calculate SNR_{in}^2 leads to a DQE value of unity for an ideal energy-integrating detector – a detector that absorbs all the energy from the incoming photons without adding noise – something that would not be true if SNR_{in}^2 had not been energy weighted.

The difference between the energy-weighted SNR, given by Eq. (2.25), and the non-weighted SNR is typically only a few percent for most clinically used beam qualities; the energy-weighted SNR being smaller [100]. However, if the DQE concept is expanded to the efficiency of a detector to discriminate a signal from the background in a specific detection task, the ideal photon-counting detector described above is no longer optimal. A detector that only counts photons will lose some of the information available in a poly-energetic radiation beam, and must also consider the energy of each photon to be ideal [100]. That is, each photon must be given a weighting factor dependent on the task. The ideal detector will then depend on the energy spectra of the signal and the background and hence on the specific object and beam quality. This further complicates the matter of normalizing DQE, and different ways of addressing the problem are conceivable.

1) Comparing the detector with an ideal detector that detects information in the same way leads to a DQE between 0 and 1 for all detectors. Obtaining an efficiency measure for detectors with a fixed maximum value of unity was the purpose of introducing the DQE. However, two different types of detectors with the same DQE may then perform differently.

2) Comparing the detector with a photon-counting detector results in an energy-integrating detector never being able to reach a DQE of 100%, which may be motivated since the energy integration is non-ideal. However, it can then be argued that the DQE concept is not adapted, only adopted, for energy-integrating detectors.

3) As pointed out, the introduction of the task-dependent DQE results in non-unique normalization and further complicates the matter. Nevertheless, if the imaging detector is to be compared with an ideal detector, which is truly ideal, the DQE should have a maximum value of unity. On the other hand, changing the properties of the ideal detector for each specific task is not practical since the difficulty in comparing the DQE of different detectors would then increase dramatically.

Although further investigations concerning the task-dependent DQE have been performed [101], and the use of detectors that employ ideal energy weighting to normalize the DQE has been proposed for mammography [102], the more general way of defining the ideal detector, as either photon counting or energy integrating, is still the most common solution to the problem of normalizing the DQE. In this work, SNR_{in}^2 was determined according to Eq. (2.25), *i.e.* each quantum is weighted by its energy. A spectrum-simulating program [103] was used to calculate q(E) per unit K_{air} for the beam qualities used. K_{air} was determined with a solid state detector insensitive to backscattering (R100, RTI Electronics, Mölndal, Sweden) connected to an electrometer (Solidose 300, RTI Electronics, Mölndal, Sweden). The detector was calibrated against an ionization chamber traceable to BIPM (Bureau International des Poids et Mesures, Sèvres, France) at several different beam qualities (tube voltage, equivalent filtration: 50 kV_P, 9 mm Al; 70 kV_P, 21 mm Al; 90 kV_P, 29 mm Al; 117 kV_P, 39 mm Al; 141 kV_P, 19 mm Al). Linear interpolation of the calibration factor for the ionization chamber, based on the mean energy of the spectrum, was used for beam qualities at which the ionization chamber had not been calibrated. At the few beam qualities used for which the solid state detector was not calibrated against the ionization chamber, the calibration factor for the closest calibrated beam quality was used. Inspection of the different calibration factors and the energy response of the detector led to the conclusion that the error introduced by this procedure was within a few percent.

2.7.4 The DQE of a digital radiographic system

As previously mentioned, the digital MTF is not a good measure of the MTF of a digital radiographic system due to its variation with phase if the system is undersampled. The presampling MTF has therefore been introduced as a measure that is not phase dependent. Using the presampling MTF when determining the DQE has also been accepted and is the most common method [10,36,37,39-41,44,84,87,94,96]. The DQE of a digital radiographic system can therefore be expressed as:

$$DQE(u,v) = \frac{MTF_{pre}^2(u,v)}{NNPS(u,v)SNR_{in}^2}. \tag{2.26}$$

However, some authors have used the expectation MTF (EMTF) when determining the DQE [33,38]. The EMTF is the expectation value of the digital MTF, averaged over all phases [65]. If the amount of aliasing in the system is relatively small, the expectation MTF is similar to the presampling MTF [65], but a difference at frequencies close to the Nyquist frequency has been observed [89]. The use of the EMTF can be motivated by the fact that, when determining the DQE, a sampled representation of the noise is used and that the signal should therefore also be sampled. However, the similarity of the EMTF to the presampling MTF is probably the reason why, in more recent years, the use of the presampling MTF has dominated. In the present work, the presampling MTF was used for all determinations of the DQE.

Thus, by using either the presampling MTF (insensitive to aliasing) or the expectation MTF (averaging out the effects of aliasing) in combination with the digital NPS (for which the expectation value in the definition leads to a measure of the noise properties of the system that is not phase dependent), a relevant measure of the DQE of a digital radiographic system can be obtained based on concepts developed from linear-systems theory for stationary systems, although the system itself is neither stationary nor linear. Not only is the DQE relevant for digital radiographic systems, but also of greater importance than for screen/film systems since, as pointed out by Moy [104], the MTF is not the best quantity to describe the resolution properties of a digital imaging system, but rather the DQE. Since the image produced is in digital form, the modulation of frequencies can be altered by image processing and the MTF therefore loses its meaning as a description of the modulation alteration of the system. The SNR of a specific frequency is, however, unaltered by stationary linear image processing, such as low-pass or high-pass filtering, and the DQE of the system, if the image processing is included, is therefore unaffected by such image processing. The MTF is still a very important measure of the imaging detector since any real system has additional noise sources, meaning that a high detector MTF increases the possibility of obtaining a high DQE.

2.7.5 Determining the DQE of a digital radiographic system

Equation (2.26) can be used to determine the DQE of a digital radiographic system experimentally. To obtain the values of the quantities on the right-hand side of the equation, the methods described above can be used. As stated previously, one-dimensional representations of the MTF and the NPS are most often used, and hence a one-dimensional DQE is obtained. This is somewhat unsatisfactory since the DQE may vary in different directions. The presampling MTF of an undersampled digital system may be rotationally asymmetric, and the NPS of such a system will inevitably vary with the direction, due to aliasing of the noise. To increase the validity of the determination, the DQE is often determined in two orthogonal directions – close to the coordinate axes – and then either averaged and presented as an average DQE of the system or presented separately for the two directions.

Due to, for example, the heel effect and the divergence of the radiation beam, the assumption of white noise in the input signal used for collecting flat-field images for determining the NPS – and hence a constant value of $\mathrm{SNR}_{\mathrm{in}}^2(u,v)$ for all frequencies – is not entirely true. The inhomogeneity in the radiation field caused by the above mentioned effects lead to a lower $\mathrm{SNR}_{\mathrm{in}}^2$ for low spatial frequencies. However, a correction for non-homogeneity of the X-ray beam is usually applied by some sort of background trend adjustment of the image used for the NPS determination. (Hence, the correction is applied to the output SNR, although it is the result of an error in the input SNR.) A common method is to fit a low-order polynomial surface to each ROI and then subtract this surface from the data in order to "detrend" the ROI [66]. When using this technique, it is important that the average pixel value of the ROI is left unaltered, as the NNPS will be erroneously determined otherwise. In the present work, a second-order polynomial surface was used to detrend the ROIs used for the NPS determinations. However, in Paper IV no correction was applied. The motivation was that the detectors evaluated used a bright map that should correct for beam inhomogeneity.

2.7.6 Standardized determination of the DQE

Although not explicitly stated in Eq. (2.26), the DQE is dependent on a number of different parameters describing the conditions of exposure, including the beam quality and dose level used. DQE determinations of digital radiographic systems have been performed in many different ways, and there is yet no standardized way of performing the measurements. Differences in the methods used are not only those addressed here regarding determination of the MTF, the NPS and the SNR_{in}, but also the beam quality, the dose level and the frequency resolution used, and so on. This results in a large variation in DQE results, and it is difficult to judge their validity and reliability. However, the International Electrotechnical Commission (IEC) is working on a standard for determining the DQE of digital radiographic systems.[†] The standard has not yet been approved, but is in an advanced stage of preparation (May 2003). If the published standard is followed, it will simplify the comparison of DQE determinations performed by different research groups on different systems.

2.7.7 Modelling the DQE

Several authors have used a theoretical approach to LSA by modelling quantities such as the MTF, NPS and DQE of complete hypothetical or real digital radiographic systems or specific components [11,12,26,29,95,105-115]. Theoretical LSA can be very useful at the design stage since it may reveal weaknesses in a system and can be used to optimize parameters. The DQE models are often very complex, incorporating a complete theoretical description of the signal and noise propagation of every stage in the imaging chain, where each stage is characterized by its gain, blurring, aliasing or addition of noise. Such modelling is usually termed cascaded linear systems analysis, since the imaging system is modelled as a cascade of independent linear systems, or stages, where each stage represents a physical process.

A DQE model used in this work was developed by Hejazi and Trauernicht [26]. The model expresses the paraxial DQE of a lens-based radiography system as:

[†] IEC project 62220-1 Ed. 1.0: Medical electrical equipment – Characteristics of digital X-ray imaging devices – Part 1: Determination of the detective quantum efficiency

$$DQE(\varphi,u)=\frac{\alpha}{1+\frac{1-I}{I}+\frac{1}{g_{scn}\eta_{CCD}\eta_{L}MTF^{2}(u)}\left(1+\frac{n_r^2+n_e^2+\frac{tq_d}{m^2}}{\alpha g_{scn}\eta_{CCD}\eta_{L}\varphi}\right)}, \tag{2.27}$$

where the lens coupling efficiency, η_L, is given by:

$$\eta_L=\frac{T_L}{1+4f_{\#}^2(1+m)^2}. \tag{2.28}$$

The other parameters are: X-ray absorption, α; Swank factor, I; screen gain, g_{scn}; CCD quantum efficiency, η_{CCD}; readout noise, n_r; other electronic noise, n_e; integration time, t; dark current, q_d; demagnification, m; X-ray output, φ; lens transmission factor, T_L and *f* number of the system (the focal length divided by the aperture of the lens [116]), $f_{\#}$. (See Hejazi and Trauernicht [26] for a more thorough explanation of the parameters.) Equation (2.27) was used to calculate the DQE of two model systems similar to two systems evaluated experimentally (Paper IV). All data on the real systems were not known, leading to the use of typical values for some of the parameters (Paper IV, Table 2).

Due to the Poisson distribution of quanta, the number of quanta present at each stage of an imaging system is of importance. Each new stage in the imaging chain reduces the DQE [108], but as long as the number of quanta present at a certain stage is higher than the number of X-ray photons initially detected (the 'primary quantum sink') by at least an order of magnitude, the reduction in the DQE due to this stage is small [29]. The term 'secondary quantum sink' is used for a stage at which the number of quanta is lower than the number of detected X-ray photons. Such a stage will effectively limit the DQE of the system. A graph of the number of quanta present at each stage in the imaging chain is usually called a quantum accounting diagram (QAD) and can be used to analyse weaknesses in the construction of an imaging system. For the two modelled systems described in Paper IV, QADs were produced.

2.7.8 Uncertainties in DQE determination

Regarding uncertainties in measurements of the presampling MTF with the tilted slit method, systematic errors are the predominant source. From an image of a slit of length 3 cm, as was used in the present work, typically 5-20 realizations of the presampling MTF are obtained, depending on the angle of the slit relative to the sampling coordinates and the pixel size. The relative standard error in the average presampling MTF at any given frequency is then typically smaller than 1%. However, the uncertainty due to, above all, the extrapolation of the noisy tails of the LSF is substantially higher. If care is not taken, the extrapolation may induce an error of several percent in the MTF. Since the MTF is squared when calculating the DQE, this error may heavily influence the accuracy of the DQE measurement. The extrapolation also removes a possible low-frequency drop, further increasing the systematic error. Other uncertainties in the DQE are caused by the determination of SNR_{in}^2, the measurement of the NPS and the linearization of the system. No detailed analysis of the uncertainty in the DQE results presented in this thesis was performed, since there is no accepted method of estimating the uncertainty in DQE determinations.

2.8 Determining the two-dimensional DQE (Paper III)

As has already been mentioned, DQEs have been determined for digital radiographic systems in a one-dimensional manner. However, since these systems cannot be assumed to be isotropic, a two-dimensional measure of the imaging properties is needed. The aperture mask method presented in Paper II for determining the two-dimensional presampling MTF was therefore further developed (Paper III) to enable the determination of the two-dimensional DQE over the entire frequency domain for a digital radiographic system. Due to the large hole size used in the aperture mask, the two-dimensional presampling MTF could only be determined up to a frequency of approximately 2.3 mm^{-1} in the study described in Paper II. This was a combined result of the large correction applied for the finite hole size and the imperfection in the positioning of the holes of the aperture mask perpendicularly to the X-ray beam (leading to a large uncertainty in F in Eq. (2.17)). Nonetheless, the one-dimensional presampling MTF in a specific direction could be determined up to the Nyquist frequency when the disk radius used for the correction was optimized specifically for that direction. However, a complete measure of the two-dimensional presampling MTF and the DQE up to the Nyquist frequency was desirable, and a new aperture mask was therefore constructed with substantially smaller holes for the study described in Paper III. One hundred holes were produced in a 10×10 matrix, with a separation of 7 mm, in 0.65 mm thick lead foil using a drill of diameter 0.1 mm. The lead was attached to approximately 4 mm of poly(methyl methacrylate) (PMMA) for support. (See Paper III for a complete description of the manufacturing process.)

The new aperture mask was used to determine the two-dimensional presampling MTF and DQE of a CR system, the Agfa ADC Compact Plus (Agfa-Gevaert, Mortsel, Belgium) using MD30 image plates read in high-resolution mode (sampling distance 0.1 mm). Images of the aperture mask, adjusted to be perpendicular to the radiation in the centre of the mask, were collected at a beam quality given by a tube voltage of 70 kV_P and a total filtration equivalent of 9 mm of Al with a distance of 205 cm between the focal spot and the detector. Flat-field images were collected at the same beam quality at a K_{air} of 5.0 μGy for determination of the NPS. Since the two-dimensional NPS was to be used in the calculations, no frequency averaging to reduce the statistical uncertainty could be applied, and a large number (64) of flat-field images were therefore collected for ensemble and spatial averaging. As previously described, each image was divided into ROIs measuring 128×128 pixels and the NNPS was calculated for each of these ROIs. The ROIs were shifted between each image so that no two ROIs were positioned at the same place.

The two-dimensional presampling MTF was obtained in a way similar to that described in Paper II, although methodological differences existed due to the new aperture mask. Due to the small hole size, the aperture mask had to be relatively thin in order to keep the partial occlusion at a reasonable level. This led to penetration of radiation through the aperture mask which, in combination with the decreased signal resulting from the smaller holes, led to a substantial amount of background. The background had to be subtracted from each DSF, and this was the reason why the holes were positioned further apart in the aperture mask used for the study described in Paper III. The background subtraction was performed by fitting a first-order polynomial surface to the data belonging to each DSF situated more than 4.0 mm from the centre of the DSF, and then subtracting the fitted surface from the DSF. To find the phase of each hole relative to the sampling coordinates, each DSF was integrated in the scan and subscan directions. For the integration in each of the directions, data at a distance less than 0.5 mm from the central line in the orthogonal direction were used. Using only the central line led to too high a noise level, as did the use of integration of the entire DSF. Using data within an area of 7×1 mm^2 in this way was found to be a good compromise, since the central part of the DSF was included whereas the noisy tails were excluded. No normalization of the DSFs was employed, since it was found that such a process resulted in an ill-shaped finely sampled DSF. The DSF was then resampled by linear interpolation to obtain a finely sampled DSF with equidistant sampling. The sampling distance of the resampled DSF was 0.01 mm in each direction, corresponding to one tenth of the sampling distance of the system.

In order to eliminate the noisy tails, the resampled DSF was extrapolated exponentially below the 0.1% level. As discussed previously, the extrapolation procedure commonly used with the tilted slit method introduces a systematic error, but reduces stochastic uncertainties. The use of the 1% level for the aperture mask method – the level used for the tilted slit method – led to an overestimation of the presampling MTF, especially at low frequencies. An extrapolation level that resulted in agreement between the two methods at the lowest frequencies (<0.2 mm^{-1}) – the frequencies at which the extrapolation procedure has the largest influence on the result – was therefore chosen. Before extrapolation, a 9×9 smoothing filter (boxcar) was applied to the resampled DSF to reduce the noise.

In order to increase the frequency resolution and to match the frequency resolution of the NNPS, the resampled DSF was placed in an array of size 2560×2560, the remainder of the array being padded with zeroes. The resampled DSF was then

Fourier transformed and corrected for the finite size of the holes and the smoothing applied to the resampled DSF. The former could not be performed in the semi-empirical manner described in Paper II since the presampling MTF was virtually zero at the frequency of the first zero value of the Bessel function used in the correction. The diameters of the holes were therefore determined using a video measuring system (SmartScope ZIP 400, Optical Gaging Products, Inc., Rochester, NY, USA) and the average hole diameter was found to be 0.105±0.002 mm (±1 SD). The diameter of the disk used for the correction was 0.101 mm – the effective average diameter of the holes assuming 100% attenuation and taking into account the effect of partial occlusion [117]. Regarding the smoothing of the resampled DSF, smoothing a signal with a two-dimensional boxcar filter is equivalent to convolution with two orthogonal rect functions, corresponding in frequency space to multiplication by two orthogonal sinc functions [118]. Correction for the smoothing was therefore performed by dividing the two-dimensional presampling MTF by the two sinc functions corresponding to the boxcar filter.

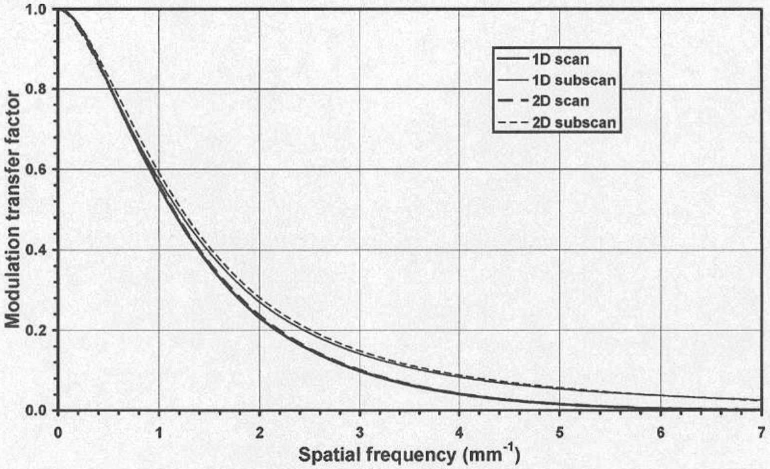

Figure 2.15. Presampling MTF of the Agfa ADC Compact Plus in directions close to the scan and subscan directions obtained with the tilted slit method (1D) and the aperture mask method (2D). (From Paper III.)

The smaller hole size enabled the determination of the two-dimensional presampling MTF up to the Nyquist frequency, and the two-dimensional DQE was calculated according to Eq. (2.26). The aperture mask method was compared with the tilted slit method for determining the one-dimensional presampling MTF, and good agreement was found (Fig. 2.15). The two methods agreed to within ±3% up to the Nyquist frequency (5 mm^{-1}). Figure 2.16 shows the two-dimensional presampling MTF, NNPS and DQE of the Agfa ADC Compact Plus at $K_{air} = 5.0$ μGy. The DQE is somewhat more symmetric than the presampling MTF, since some of the asymmetry is cancelled by the NNPS, which contains quantum noise filtered by the MTF. For both the NNPS and the DQE, data at frequencies lower than or equal to 0.1 mm^{-1} have been excluded due to their poor reliability and validity.

After confirming that the presampling MTF was determined in a manner consistent with the tilted slit method, the two-dimensional DQE was radially averaged to obtain a relevant one-dimensional measure of the DQE. This DQE was compared with the averaged DQE achieved by averaging one-dimensional determinations of the DQE in orthogonal directions, as is usually done. The one-dimensional noise power spectra used for the one-dimensional DQE determinations were calculated in two different ways, using both the method of axial averaging (4 lines on each side of the axis; band method) and radial averaging (a 90° sector around the axis; sector method). A slice of the two-dimensional presampling MTF obtained with the aperture mask method was used for the one-dimensional DQE determinations to decrease the uncertainty due to the determination of the presampling MTF. The results are presented in Fig. 2.17. It is evident that the two one-dimensional methods of obtaining an average DQE agreed well with the radially averaged two-dimensional DQE. The band method resulted in an average DQE that was more or less identical to the radially averaged two-dimensional DQE, but has the drawback that the DQE can only be determined up to the Nyquist frequency along the axes (5 mm^{-1}). The sector method can be used to determine the average DQE up to the highest relevant frequency (Nyquist frequency along the diagonal of the coordinate system; $5\sqrt{2}$ mm^{-1}), but a deviation was observed above 5 mm^{-1}. However, this deviation was very small in absolute numbers.

For the CR system evaluated here, the presampling MTF and the DQE were highest in the subscan direction and decreased towards the scan direction, where the lowest values of these quantities were found. This explains the good agreement found between the radially averaged two-dimensional DQE and the average DQE obtained from one-dimensional DQE determinations along the axes. Albert and Maidment [118] performed a theoretical determination of the presampling MTF and DQE in different directions for model systems, and presented results for an "alias-free" model – a detector for which the presampling MTF above the Nyquist frequency is low – which had a square sampling aperture and an exponentially decaying transfer function describing the spread of the signal due to interaction processes, for which the DQE along the diagonal was substantially higher than that along the coordinate axes at high frequencies. For such a detector, the average DQE obtained from one-dimensional DQE determinations along the axes would not result in a correct measure of the average DQE behaviour of the system. The good agreement found for the CR system in the study described in Paper III can therefore not be assumed to be valid in general for digital radiographic systems. Unless a specific system has been shown to be isotropic, a two-dimensional representation of the imaging properties should therefore be used if the system is to be described in detail.

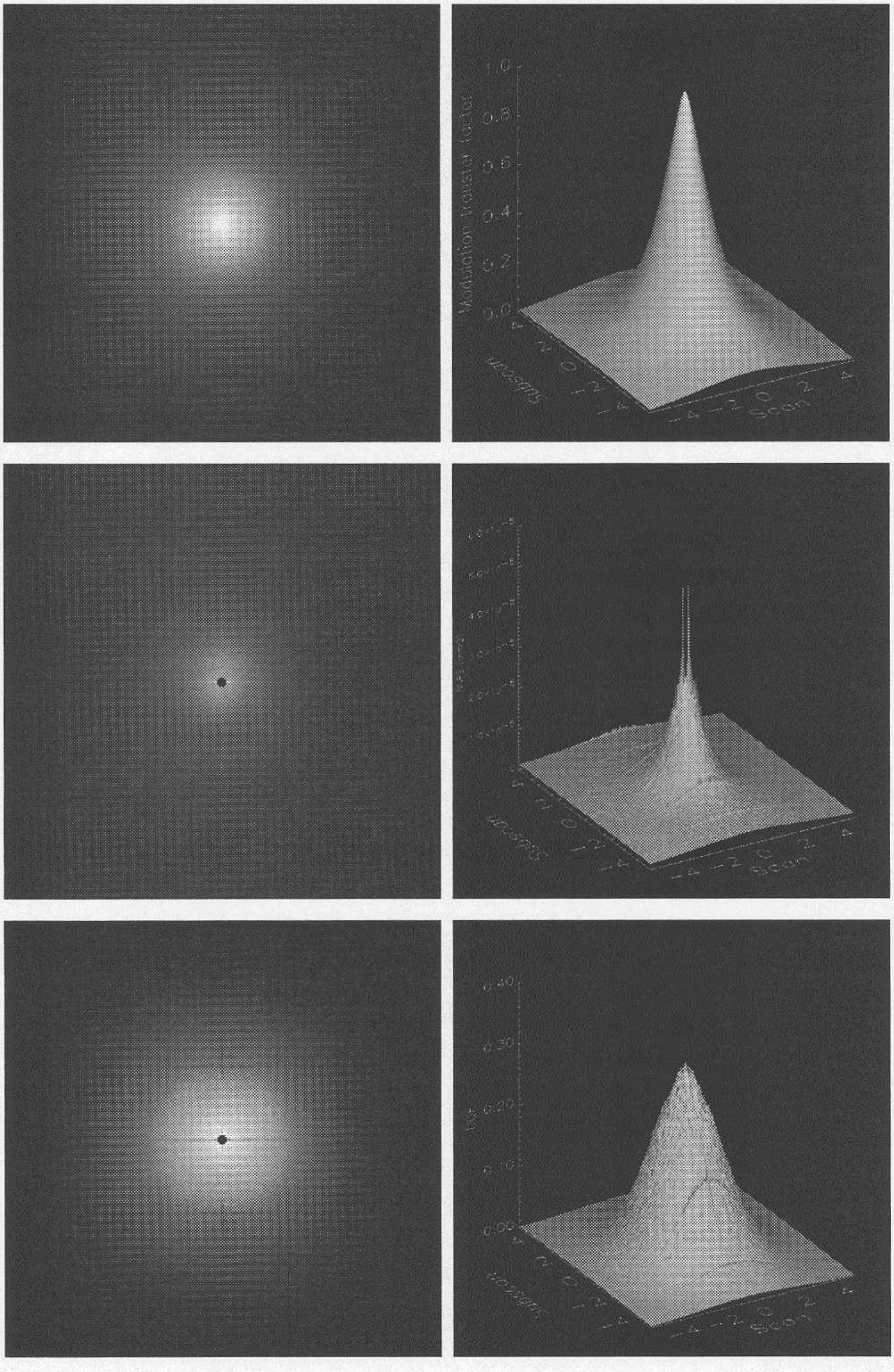
Modulation transfer factor
1.0
0.8
0.6
0.4
0.2
0.0
4
2
0
-2
-4
Subscan
-4
-2
0
2
4
Scan
6.0×10^{-8}
5.0×10^{-8}
4.0×10^{-8}
3.0×10^{-8}
2.0×10^{-8}
1.0×10^{-8}
4
2
0
-2
-4
Subscan
-4
-2
0
2
4
Scan
0.40
0.30
0.20
0.10
0.00
4
2
0
-2
-4
Subscan
-4
-2
0
2
4
Scan

Figure 2.16. (Opposite page.) Two-dimensional presampling MTF (top), NNPS, and DQE (bottom) of the Agfa ADC Compact Plus at K_{air} = 5.0 μGy. The data cover the entire frequency domain, ranging from a spatial frequency of -5 mm^{-1} to 5 mm^{-1} along the axes. Data at frequencies lower than or equal to 0.1 mm^{-1} are excluded for the NNPS and the DQE. Tube voltage = 70 kV_p and total filtration equivalent of 9 mm Al. (From Paper III.)

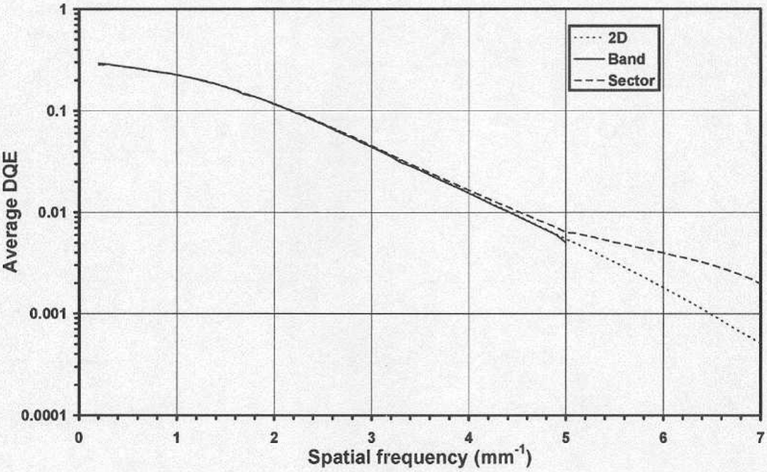

Figure 2.17. Average DQE obtained as the radial average of the two-dimensional DQE (2D) and as the average of the one-dimensional DQE in the scan and subscan directions using the band and sector methods. (From Paper III.)

2.9 Evaluation of two generations of a CCD-based DR system (Paper IV)

The aim of the study presented in Paper IV was to evaluate the imaging properties of two generations of a CCD-based DR system manufactured by IMIX ADR Oy (Tampere, Finland), the IMIX and the IMIX 2000. The thorax versions – floor-mounted chest stands – were used. Both experimental determination of quantities such as presampling MTF, NNPS, NEQ and DQE and a semi-theoretical determination of the DQE of two systems similar to the IMIX (System A) and the IMIX 2000 (System B) (Paper IV, Table II), based on the model by Hejazi and Trauernicht [26] (Eq. (2.27)), were performed. QADs for the two model systems were also produced. The experimental determinations were performed over a wide range of K_{air} values and, for the IMIX 2000, at several different beam qualities (Paper IV, Table I). The tilted slit method was used for the determination of the presampling MTF, and the one-dimensional NNPS used for DQE determination was obtained by radial averaging within a 90° sector of the two-dimensional NNPS.

It was found that the IMIX 2000 was substantially improved compared with the IMIX. The presampling MTF of the IMIX showed a large variation over the detector surface, a phenomenon which was much smaller in the IMIX 2000 (Fig. 2.18). Although the central presampling MTFs of the two systems were similar, the peripheral MTF of the IMIX was much lower than that of the IMIX 2000. The non-homogeneous response of the IMIX was also visible in SNR surfaces, obtained as the average pixel value divided by the standard deviation of ROIs of size 40×40 pixels (Fig. 2.19). The SNR dropped dramatically at the periphery of the detector surface for the IMIX, while the decrease for the IMIX 2000 was much lower.

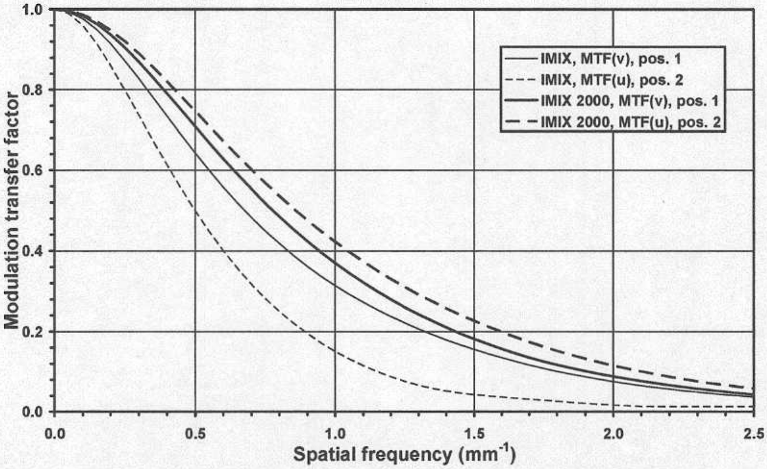

Figure 2.18. Presampling MTFs of the IMIX and the IMIX 2000 determined centrally (pos. 1) in the vertical direction and peripherally (pos. 2) in the horizontal direction at 70 kV$_P$. (Redrawn from Paper IV.)

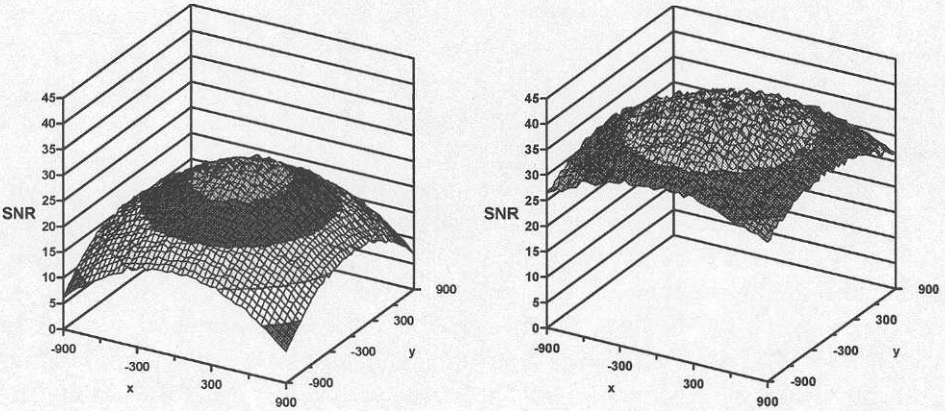

Figure 2.19. SNR surfaces for the IMIX (a) and the IMIX 2000 (b) at an interpolated K_{air} of 5 μGy at 70 kV$_P$. Each point represents the SNR of an ROI of size 40×40 pixels, located at the position described by the x- and y-axes. (Redrawn from Paper IV.)

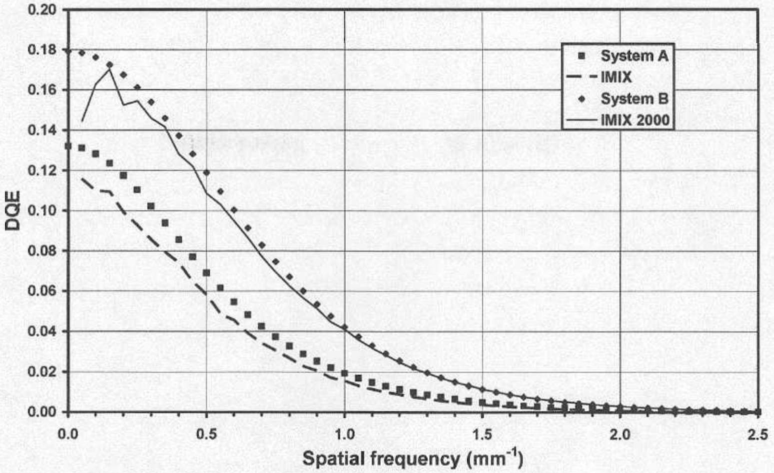

Figure 2.20. Experimentally determined DQE of the IMIX and the IMIX 2000 and modelled DQE of systems similar to the IMIX (System A) and the IMIX 2000 (System B) at K_{air} = 50 µGy at 70 kV_P.

The DQE of the IMIX 2000 was substantially improved compared with the IMIX. Figure 2.20 presents the experimentally determined DQE for the IMIX (vertical direction only) and the IMIX 2000 (average of both directions) and the calculated DQE of the two modelled systems at K_{air} = 50 µGy at 70 kV_P. The experimentally determined central presampling MTFs were used for the calculations of the model systems. The agreement between the IMIX 2000 and System B was very good, whereas a difference between the IMIX and System A can be observed. At lower K_{air} values, the difference between the real systems and the model systems was larger (Paper IV, Figs. 6 and 9), probably due to underestimation of additive noise sources by the model.

The QADs produced for the two model systems revealed the existence of a secondary quantum sink for both systems (Fig. 2.21). In spite of the difference in DQE found between the IMIX and System A, the agreement between the DQE curves obtained for the model systems and the real systems was good enough to conclude that the models described the real systems with sufficient precision. Thus, it is reasonable to conclude that the IMIX and the IMIX 2000 suffer from secondary quantum sinks, partly explaining the relatively low DQE values observed experimentally.

The dependence on the beam quality for the DQE of the IMIX 2000 was found to be small (Fig. 2.22). This could possibly be explained by the secondary quantum sink. For a system without a secondary quantum sink, it is probable that the lower absorption of photons with higher energies would result in a lower DQE at high tube voltages, since the primary quantum sink would be deeper. However, with the existence of a secondary quantum sink, the increase in the number of secondary quanta emitted after absorption of a photon with higher energy counteracts the effect of the deeper primary quantum sink in such a way that the secondary quantum sink is not deepened to the same extent as the primary quantum sink. Since the deepest quantum sink influences the DQE most, the decrease in DQE at higher energies should therefore be smaller for a system with a secondary quantum sink.

The central presampling MTF was only determined in the vertical direction on the IMIX. Due to a mistake during data handling, NNPS data in the horizontal direction were used for the determination of the DQE in Paper III. This has been corrected in the results presented here. However, as can be seen by comparing Fig. 2.22 with Fig. 7 in Paper III, the effects of the error were minor.

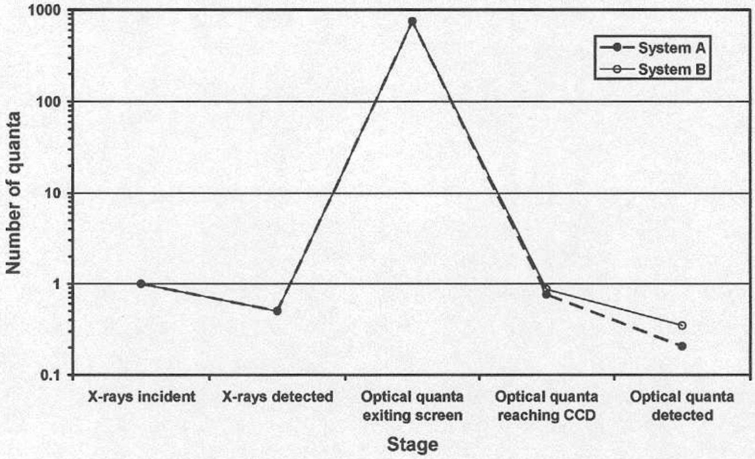

Figure 2.21. Quantum-accounting diagram for the systems similar to IMIX (System A) and IMIX 2000 (System B) at 70 kV_P. (Redrawn from Paper IV.)

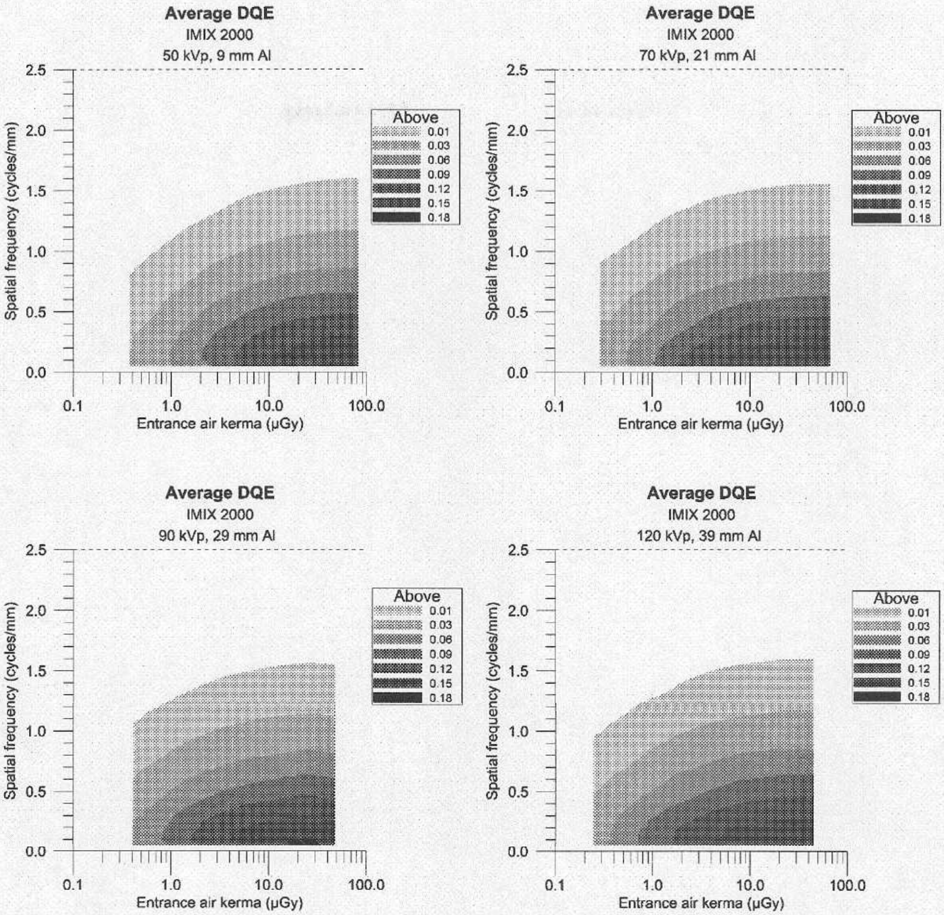

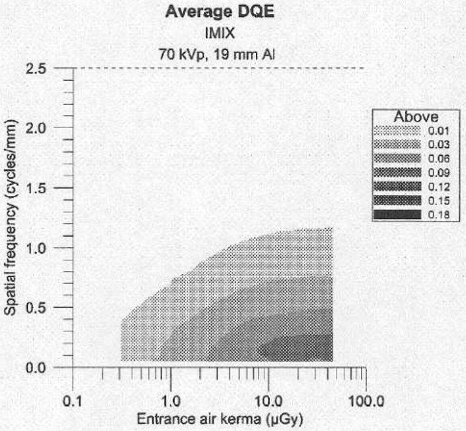

Figure 2.22. Average DQE as a function of spatial frequency and entrance air kerma for the IMIX (only vertical direction) and IMIX 2000 at different beam qualities. In order to obtain a smoother image, each DQE value was averaged with its nearest neighbours.

3. Clinical System Performance

3.1 Operationalization – or: What was actually measured?

Operationalization is the process of defining measurable variables thought to describe the phenomenon which is the subject of study. The operationalization process is of the utmost importance in any scientific task since the reliability and validity of the results from a study are strongly connected to the success of the operationalization. The reliability describes the precision of the measurement; a high reliability demanding small stochastic errors. The validity describes how well the variables describe the phenomenon, meaning that a high validity requires a small systematic error. Successful operationalization therefore requires both high validity and high reliability.

Image quality in radiography is a phenomenon of enormous complexity. It is extremely task dependent – the demands on noise level, resolution and contrast differing from discipline to discipline. It also involves many processes that are not fully understood and described, such as image processing and signal detection and interpretation by the human observer. It is therefore easy to understand the difficulty in defining a general image quality measure with high validity. On the other hand, a measure with high validity for a specific task has the inherent property of being less generalizable. This difficulty in performing successful operationalization for an image quality measure has led to the diverse methods of evaluating image quality or system performance in use today [54,55].

There is a danger in mixing the concepts of validity and reliability in such a way that one is led to believe that they are in any way connected. The reliability of a measurement can be very high, but the validity still non-existent if conclusions are drawn about a phenomenon the measure does not describe. This is especially poignant in medical imaging. An example is the use of linear-systems analysis to evaluate system performance by describing the imaging properties of an imaging system through the use of the quantity DQE. This quantity can be determined with a high reliability and the validity in terms of systematic errors is acceptable, as is discussed elsewhere in this thesis. However, if the results are used to draw conclusions about phenomena other than that used as the basis for the original operationalization, namely the transfer of SNR, the validity is naturally immediately reduced. Using DQE as a measure of the clinical performance of a system, or NEQ as a measure of the clinical image quality, without establishing the relationship between these quantities and measures taking into account the complete imaging chain, involving image processing, display and the response of the observer (cf. Paper V, Fig. 1), is therefore an approach with low validity. The DQE should not be underestimated since the imaging properties of the detector constitute an important link in the imaging chain. However, in situations where the clinical image quality is more affected by disturbing anatomical structure than by quantum noise and system noise, the DQE is a less important parameter. There is therefore a risk of overestimating the importance of the DQE in such a way that it is assumed that a system with a higher DQE always results in higher clinical image quality. The validity of DQE must be assessed in all clinical situations if it is to be used as a measure of clinical system performance.

3.2 Evaluation of image quality

3.2.1 An introductory example and a global concept of image quality

The practical use of a concept such as DQE is based on the requirements of linearity and stationarity, which lead to a simplified description of the imaging system. However, such approaches cannot be used for clinical image quality and every new situation has to be treated as a special case if all the processes involved are not understood. It goes without saying that the clinical performance of an imaging system in a specific imaging task can not immediately be transferred to another imaging task.

Different approaches to assessing image quality have been employed. Verdun *et al.* [119] proposed an image quality index (IQI) for chest radiography based on three requirements on a global concept of image quality:

1) Image quality must be represented by a single number in order to simplify comparisons.

2) This number must characterize the entire radiological system, including beam quality, and geometry.

3) The experimental procedure should be simple and should allow testing of a large number of installations or materials.

The IQI is defined as the smallest detectable sphere with a 2% false-negative probability [119]. Using such an approach is appealing because it fulfils the requirements stated above, although the validity of such an approach can be questioned if it is based on non-anthropomorphic phantoms. Burgess *et al.* [120] found that in digital mammograms, the threshold contrast for a number of extracted masses increased with the size of the masses, a result which was explained by an increase in the anatomical structure at low frequencies. The same experiment conducted in a homogenous background would lead to the opposite result. This difference shows the low general validity of using results from test phantom studies to predict the outcome of clinical tasks. In chest radiography it has also been stated that the quantum noise is of minor importance and the anatomical structure plays a major role in detection (chest radiography is quantum saturated) [121,122]. The general validity of methods for evaluating clinical image quality that do not take the anatomical structure into account can therefore not be assumed to be high for chest radiography.

3.2.2 Grading of visibility of details

A different approach to assessing image quality is to use grading of visibility of details in an image. Performing such a study in a controlled scientific manner is usually termed visual grading analysis (VGA). VGA can either be performed in a relative manner, where each image is compared to a reference image and the observer states whether the details in the image are reproduced better or worse than in the reference image, or in an absolute manner, where the observer gives a statement about the visibility of each detail on an absolute scale. Both variants can be used to assess the image quality of clinical images if expert radiologists are used as observers and the visibility of relevant structures is graded. Examples of typical rating scales for relative and absolute VGA, which were used in the study described in Paper V, are presented in Tables 3.1 and 3.2, respectively. Thorough investigations of VGA for assessing clinical image quality have been performed [54,123].

Table 3.1. The rating scale used for relative VGA study presented in Paper V.

Relative rating:	**Meaning**
	The reproduction of the structure in the image is
-2:	*much worse than*
-1:	*worse than*
0:	*the same as*
+1:	*better than*
+2:	*much better than*
	the reproduction of the corresponding structure in the reference image

Table 3.2. The rating scale used for absolute VGA study presented in Paper V.

Absolute rating:	**Meaning**
	The structure in the image is
1:	*not visible*
2:	*poorly reproduced*
3:	*adequately reproduced*
4:	*very well reproduced*

For the analysis of the data collected in a VGA study, the numerical values of the ratings are often used. Attributing quantitative properties in this way to the originally qualitative (ordinal) scales can be questioned [124]. The method was used here (Paper V) mainly because it is common [23,49-52,54,55,119,123,125-136] (a somewhat questionable justification) and accepted by some statisticians. By accepting the numerical values of the gradings, a relative visual grading analysis score ($VGAS_{rel}$) and an absolute visual grading analysis score ($VGAS_{abs}$) can be calculated. One expression of the $VGAS_{rel}$, which was used in Paper V, is:

$$VGAS_{rel} = \frac{\sum_{i=1}^{I}\sum_{s=1}^{S}\sum_{o=1}^{O}[-1]\cdot G_{(rel)o,i,c}}{ISO}, \tag{3.1}$$

while the $VGAS_{abs}$ was calculated as:

$$VGAS_{abs} = \frac{\sum_{i=1}^{I}\sum_{s=1}^{S}\sum_{o=1}^{O} G_{(abs)o,i,c}}{ISO}. \tag{3.2}$$

In Eqs. (3.1) and (3.2), $G_{(rel)o,i,c}$ is the relative rating and $G_{(abs)o,i,c}$ is the absolute rating for a particular image (i), structure (s) and observer (o). I, S and O are the number of images, structures and observers, respectively, used for each system in the study. The term [-1] in Eq. (3.1) indicates that if a randomization of reference images is used, the reference image in each pair of images can be assigned the same rating as the evaluated image, but with the opposite sign. Since the actual relative rating is dependent on the quality of the reference image, the randomization of reference images may cause biased results. In order to avoid possible asymmetry caused by the number of times a given system is chosen as the reference, both images in the evaluated pair can be given a rating; the observer rates the image compared with the reference image and in the subsequent calculation process the reference image itself is given the same score with the opposite sign. Thus, $G_{(rel)o,i,c}$ is calculated with a positive sign for the image compared with the reference image and with a negative sign for the reference image itself. This procedure is based on the assumption that the grading for each pair would be of the same magnitude but with the opposite sign if the compared image and the reference image changed places. With this kind of symmetry, the average score of all systems will be zero, and the relative score for a given system will be compared with this average value. If randomization of reference images is not used, but a specific system is chosen as a reference, the [-1] term and the rating of the reference image can be omitted and a visual grading analysis score relative to the chosen reference system is obtained for each system.

3.2.3 The CEC quality criteria

The Commission of the European Communities (CEC) has defined "quality criteria" for specific X-ray examinations [137]. Criteria have been defined for six conventional examinations – chest, skull, lumbar spine, pelvis, urinary tract and breast. Similar documents have been prepared for paediatric radiography [138] and for CT [139]. These quality criteria are divided into three parts: 1) diagnostic requirements (image criteria and important image details), 2) criteria for radiation dose to the patient, and 3) example of good radiographic technique. The objectives of the guidelines based on the criteria are to achieve "adequate image quality, comparable throughout Europe" and "reasonably low radiation dose per radiograph" [137].

Fulfilment of the diagnostic requirements results in what is stated to be an image of "standard quality" [137]. The diagnostic requirements are grouped into image criteria and important image details. The former "in most cases specify important anatomical structures that should be visible on a radiograph to aid accurate diagnosis" [137]. The image criteria are therefore appropriate for use in VGA studies of clinical image quality. The latter provide "quantitative information on the minimum sizes at which important anatomical details should become visible on radiographs" [137]. However, since "some of these anatomical details may be pathological and therefore may not be present" [137], they may or may not be suitable for visual grading of normal images. In Table 3.3 the diagnostic requirements for chest radiographs (PA projection) are presented.

VGA based on the CEC image criteria or similar criteria has been used extensively [23,50-52,123,130-132,135,136]. This can be done either by using the image criteria themselves and letting the observers state whether they are fulfilled or not, or by extracting the structures from the criteria and letting the observers grade the visibility of these structures, either on an absolute or a relative scale, to obtain $VGAS_{abs}$ or $VGAS_{rel}$, respectively. The former may be used to produce an image criteria score (ICS) [123]:

$$ICS = \frac{\sum_{i=1}^{I}\sum_{c=1}^{C}\sum_{o=1}^{O} F_{i,c,o}}{ICO}, \tag{3.3}$$

where $F_{i,c,o}$ is the statement of fulfilment of criterion c in image i according to observer o (1 for 'yes', 0 for 'no'). I, C and O are the numbers of images, criteria and observers, respectively.

Table 3.3. CEC diagnostic requirements for chest radiographs (PA projection) [137].

Image criteria

1 Performed at full inspiration (as assessed by the position of the ribs above the diaphragm - either 6 anteriorly or 10 posteriorly) and with suspended respiration

2 Symmetrical reproduction of the thorax as shown by central position of the spinous process between the medial ends of the clavicles

3 Medial border of the scapulae to be outside of the lung fields

4 Reproduction of the whole rib cage above the diaphragm

5 Visually sharp reproduction of the vascular pattern in the whole lung, particularly the peripheral vessels

6 Visually sharp reproduction of:
  (a) the trachea and proximal bronchi,
  (b) the borders of the heart and aorta,
  (c) the diaphragm and lateral costo-phrenic angles

7 Visualization of the retrocardiac lung and the mediastinum

8 Visualization of the spine through the heart shadow

Important image details

1 Small round details in the whole lung, including the retrocardiac areas:
  high contrast: 0.7 mm diameter
  low contrast: 2 mm diameter

2 Linear and reticular details out to the lung periphery
  high contrast: 0.3 mm in width
  low contrast: 2 mm in width

3.2.4 Weaknesses of VGA

The VGASs determined according to Eqs. (3.1) and (3.2) fulfil, at least, the first two of the three requirements placed on a global concept of image quality mentioned in Section 3.2.1. However, it is questionable if a complex phenomenon such as image quality can be reduced to a single number, even if it is based on the visibility of relevant structures in a clinical image. More detail can be obtained from a visual grading study if the summation over structures is omitted and a VGAS is obtained for each structure. Since the visibility of different structures is sensitive to variations in contrast, resolution and noise in different ways, a study of the VGASs for each structure may reveal information that is hidden in the total VGAS.

The use of quality criteria for evaluating image quality can be questioned in several different ways. Commonly, healthy subjects are used for image evaluations, and it is therefore important to bear in mind that the whole idea behind VGA of image criteria is that the visibility of normal anatomy is believed to describe the ability of the system to reproduce pathological conditions, and to distinguish between normal and pathological conditions. Comparisons between VGA-based methods and more extensive methods such as ROC analysis – often referred to as the golden standard in evaluations of image quality – have been performed. Sund *et al.* [131] and Tingberg *et al.* [132] showed that the ranking of images based on visual grading of modified criteria agreed with the detection of simulated tumours in clinical images, determined using free-response forced error [140] (FFE) experiments, in chest and lumbar spine radiography, respectively, when the resolution and noise were manipulated. (FFE is an observer performance experiment related to ROC.) Under which conditions this relationship is valid remains to be investigated.

The advantage of the use of relative VGA has been stated by Tingberg [123] to be that it has a "strong separating power". However, this separating power induces two risks, both of them connected to the comparison of the two terms 'statistically significant' and 'clinically relevant'. Firstly, since the scale used is relative it is difficult to judge the clinical value of a difference between two systems. Are both systems acceptable or are both unacceptable? Secondly, there is a risk of interpreting a statistically significant result as a clinically relevant result. If enough subjects are examined, a statistically significant difference is likely to occur without this difference necessarily being clinically relevant. Since the comparison is relative, it is difficult to know how large a difference should be to be clinically relevant. When using absolute VGA or fulfilment of image criteria, the problem of statistical significance vs. clinical relevance still exists. However, since an absolute scale is used, the problem of an acceptable system is simplified. A criterion such as fulfilment of the image criteria in a certain percentage of the cases or a rating higher than or equal to 'adequately reproduced' in a percentage of the cases may be chosen for an imaging system to be acceptable.

Using fulfilment of image criteria as a basis for visual grading is perhaps the least objectionable method. It was not used in the present work, but has the advantage that the use of parametric statistics is unquestionable since the ICS – the proportion of fulfilled criteria – is the mean of a variable that can take the value of either zero or unity. The central limit theorem states that such a mean is normally distributed for large samples [141].

3.3 Comparison of DQE and VGA (Paper V)

Based on the previous discussion on the validity of DQE as a measure of clinical system performance, the aim of the study described in Paper V was to compare the imaging properties of digital radiographic systems with the clinical image quality of images produced with the systems. The study was restricted to chest radiography and to four different systems; two DR systems, the IMIX and the IMIX 2000 (IMIX ADR Oy, Tampere, Finland), and two CR systems, the Agfa ADC 70 with MD10 image plates (Agfa-Gevaert, Mortsel, Belgium) and the Fuji FCR 9501 with generation V image plates (Fuji Photo Film, Tokyo, Japan). All systems were run in standard mode, resulting in a pixel size of 0.170 mm for the Agfa ADC 70 and 0.200 mm for the others.

To determine the clinical image quality of the four systems, PA chest images of the same 23 healthy volunteers were collected with each system at 141 kV_P (total filtration equivalent of 9 mm of Al). Automatic exposure control (AEC) was used to give an average entrance air kerma corresponding to a correct chest exposure for a 200-speed screen/film system. The image processing of each system had been adjusted by application experts together with radiologists, either just before the study (for systems not clinically used at Sahlgrenska University Hospital, where the images were collected and evaluated) or during the clinical use of the system. The images were evaluated, using soft-copy reporting, by four radiologists, all of them specialists in thoracic radiology. Both absolute VGA and relative VGA were used. The structures rated were based on the European quality criteria, although modified for the study. Image criteria mainly dependent on positioning were omitted. The remaining image criteria were modified to be more precise. The criteria were finally rephrased to focus on specific anatomical details rather than the shape of general structures (Table 3.4). $VGAS_{abs}$ and $VGAS_{rel}$ were calculated according to Eqs. (3.1) and (3.2).

Table 3.4. Modified quality criteria for chest radiographs (PA projection) used in the study presented in Paper V. The shortened descriptions used for the structures are given in parentheses.

	Image criteria
1	Sharp visualization of the vessels seen 3 cm from the pleural margin (Peripheral vessels)
2	Sharp visualization of the vessels seen en face in the central area (Central vessels)
3	Visualization of the carina with main bronchi (Carina)
4	Visualization of the thoracic vertebrae behind the heart (Thoracic vertebrae)
5	Sharp visualization of the pleural margin (Pleural margin)

The significance of differences between the systems was calculated using analysis of variance (ANOVA) in conjunction with a method for multiple comparisons, the Newman-Keuls test (α=0.05), in order to reduce the risk of random significance. The statistical analysis was performed using the software STATISTICA, Release 5.1 (StatSoft, Inc., Tulsa, OK, USA).

To obtain the imaging properties of the four systems, one-dimensional presampling MTFs and the DQEs of all systems were determined along the coordinate axes. The beam quality used was 141 kV_P and a filtration equivalent of 19 mm of Al (total filtration plus added thickness of Al). Due to penetration of radiation through the jaws of the slit used for the determination of the presampling MTF, the tube voltage was lowered to 70 kV_P for the collection of slit images, which is not considered to influence the results substantially (Paper IV and Samei and Flynn [41]).

A problem occurred with the Agfa ADC 70. Apparently, the 'raw' data obtained from the system are processed in a non-linear manner. This processing cannot be prevented, which made the determination of the presampling MTF using the tilted slit method impossible. To estimate the imaging properties of the Agfa ADC 70, the presampling MTF and the DQE were therefore determined for the subsequent CR system from Agfa, the Agfa ADC Compact (Agfa-Gevaert, Mortsel, Belgium), but using the MD10 image plates used in the Agfa ADC 70. The data obtained are therefore valid for the image plate used for the clinical images, but read out in a different reader. It is possible that using these data to represent the Agfa ADC 70 leads to an overestimation of the imaging properties. The data are therefore presented as belonging to the less precise Agfa ADC.

The two CR systems (Fuji FCR 9501 and Agfa ADC) had considerably higher DQEs than the two DR systems (Fig. 3.1). The Fuji FCR 9501 had a slightly higher DQE than the Agfa ADC, and the IMIX 2000 showed an improvement compared with the IMIX, as previously discussed in Paper IV. The two CR systems were therefore deemed to be superior to the IMIX and the IMIX 2000 in preserving the SNR of the input signal, especially at high frequencies. At very low frequencies, the structured noise in the image plates in combination with the inhomogeneity of the radiation field led to a very low DQE for the CR systems, an effect not found for the DR systems due to the bright map used to correct for pixel-to-pixel variations in sensitivity. The presampling MTFs of the two CR systems were substantially higher than those of the two DR systems (Fig. 2.4).

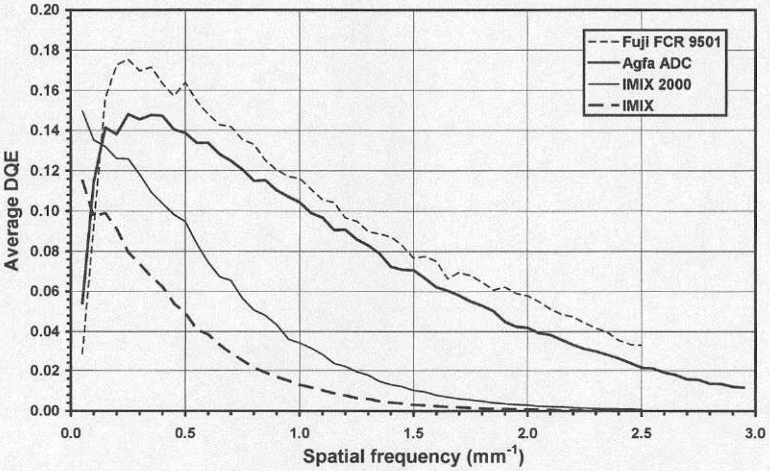

Figure 3.1. DQE at a K_{air} of approximately 5 μGy for the four systems evaluated in Paper V. Agfa ADC=Agfa ADC Compact with MD10 image plates. (From Paper V.)

For the evaluation of the clinical image quality using relative VGA, the IMIX 2000 was rated as the best system for reproducing the peripheral and the central vessels, while the Fuji FCR 9501 was rated best for the carina, the thoracic vertebrae and the pleural margin (Table 3.5). The IMIX gave the lowest scores and the Agfa ADC 70 the second lowest scores for all structures. For the total relative VGA, summed over all structures, the IMIX 2000 and the Fuji FCR 9501 could not be separated statistically, while the Agfa ADC 70 and the IMIX 2000 were placed third and fourth, respectively. The absolute VGA gave approximately the same ranking as the relative VGA. However, in the relative VGA, the differences between the systems were statistically significant for all structures, whereas in the absolute VGA, several differences were not statistically significant. For the thoracic vertebrae, the Agfa ADC 70 was also rated higher than the IMIX 2000 in the absolute VGA, whereas the opposite result was obtained in the relative VGA. For the total absolute VGA, the IMIX 2000 and the Agfa ADC 70 could not be statistically separated, while the Fuji FCR 9501 was rated highest and the IMIX lowest.

Table 3.5. VGASs for the four systems evaluated (Paper V). VGASs in the same row marked with an asterisk could not be separated statistically (Newman-Keuls, α=0.05).

	VGAS$_{abs}$				**VGAS$_{rel}$**			
	Fuji FCR 9501	IMIX 2000	Agfa ADC 70	IMIX	Fuji FCR 9501	IMIX 2000	Agfa ADC 70	IMIX
Periperal vessels	3.23*	3.26*	3.03	2.51	0.54	0.84	-0.31	-1.08
Central vessels	3.17*	3.26*	3.10	2.89	0.11	0.87	-0.28	-0.70
Carina	3.41	3.04*	3.01*	2.73	0.69	0.30	-0.26	-0.73
Thoracic vertebrae	3.43	2.63	2.95	2.36	1.01	0.21	-0.01	-1.21
Pleural margin	3.22	2.96*	2.88*	2.58	0.57	0.39	-0.09	-0.88
Total score	*3.29*	*3.03**	*2.99**	*2.61*	*0.58**	*0.52**	*-0.19*	*-0.92*

Regarding the comparison between DQE and VGA, a problem was identified; the average entrance air kerma to the volunteers was found to differ between the systems, despite the efforts to ensure that the imaging conditions were identical. As already mentioned, the DQE is a measure of the quality of the system and NEQ a measure of the quality of the image. If the same dose level is not used, a comparison between imaging properties and clinical image quality should be based on the NEQ rather than the DQE. A 'relative NEQ', taking into account the difference in exposure, was therefore determined by multiplying the DQE by the average entrance air kerma to the volunteers (Fig. 3.2).

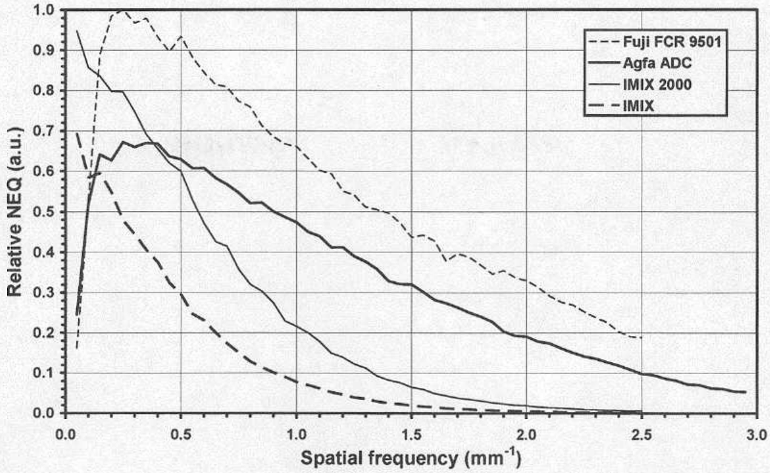

Figure 3.2. Relative NEQ for the four systems evaluated (Paper V). Agfa ADC=Agfa ADC Compact with MD10 image plates. (From Paper V.)

The Fuji FCR 9501, with a much higher relative NEQ than the IMIX 2000, produced clinical images with an image quality that was rated only slightly better. The Agfa ADC 70 produced images with lower clinical image quality than the IMIX 2000, although the relative NEQ was substantially higher for the Agfa ADC at frequencies above 0.5 mm^{-1}. As mentioned above, there is an uncertainty in the validity of applying the results of the Agfa ADC to the Agfa ADC 70. However, since the only difference is in the reader used to extract the information from the MD10 image plate, there is reason to believe that the possible overestimation is not large enough to change the result that the relative NEQ of the Agfa ADC 70 is higher than that of the IMIX 2000 at most frequencies of relevance (Fig. 3.2).

Although other factors may have influenced the results, such as differences in pixel size and grids, the results indicate that clinical performance cannot be predicted from the determination of DQE alone, and that a system with a lower DQE, under the quantum-saturated conditions in chest radiography [122], can outperform a system with a higher DQE if the image processing used on the former is more effective in presenting the information in the image to the radiologist. This result is in agreement with the findings that the quantum noise is of minor importance and that the anatomical structure plays a major role for detection in chest radiography [121]. It also exemplifies the relevance of the statement by Metz *et al.* [97]: "Hence, system rankings that are based solely on NEQ and ideal-observer performance – without regard to image display, image background, and the characteristics of human observers – must be interpreted with caution."

4. Summary and Conclusions

In this work, methods based on linear-systems theory for evaluating the imaging properties of digital radiographic systems have been addressed. The main accomplishments and knowledge gained can briefly be summarized as follows.

- A computer program for simulating the resolution properties, in terms of several different MTFs, of a digital radiographic system was developed. The program can be used to study the effects of varying detector design parameters, such as sampling distance, fill factor and size of the sampling aperture on the resulting MTFs.

- A method of determining the two-dimensional presampling MTF of a digital radiographic system – the aperture mask method – was developed. The method is consistent with the established tilted slit method in determining the one-dimensional presampling MTF. The method can be used to determine the complete SNR transfer characteristics of a digital radiographic system in term of the two-dimensional DQE.

- The imaging properties of two generations of a DR system, the IMIX and the IMIX 2000, were evaluated through experimental and theoretical LSA. The imaging properties of the IMIX 2000 have been substantially improved compared with those of its predecessor, the IMIX. However, the presampling MTF and the DQE of the IMIX 2000 are low compared with CR systems or FPDs. It is likely that both the IMIX and the IMIX 2000 involve secondary quantum sinks that limit their performance.

- The clinical performance of a digital radiographic system cannot be predicted from determination of DQE alone. A system with a lower DQE, under the quantum-saturated conditions in chest radiography, can outperform a system with a higher DQE if the image processing used on the former is more effective in presenting the information in the image to the radiologist.

5. Concluding Remarks and Future Prospects

A great challenge to medical X-ray imaging researchers lies in describing the complete imaging process – from the production of radiation via its attenuation in the human body, its detection in the imaging detector and the production of the final image from the raw image data, to interpretation by the human observer – in such a way that a grand unification theory linking human observers, model observers, Monte Carlo simulations of the imaging chain, descriptions of the image content and measures of the imaging properties of the system is obtained. Whether this is at all possible only time will tell, but if the goal is eventually reached this will not only be a scientific triumph, but will also lead to new opportunities for optimizing the use of radiation in diagnostic X-ray imaging. Every step taken in this direction is therefore an important one.

This thesis has mainly dealt with methods of characterizing the imaging properties of digital radiographic systems. As a link in the imaging chain, these properties must be appropriately described. Since the final image in projection radiography is two-dimensional, two-dimensional measures of the imaging properties are needed if a system cannot be proven to be isotropic. The introduction of two-dimensional measures will therefore hopefully lead to better descriptions of the systems. The following suggestions are proposed for the continuation of the specific work presented in this thesis.

- *Improvement of the computer program used to simulate the different MTFs of hypothetical systems.* The program could be improved by expanding the calculations to two dimensions, not demanding a square continuous sampling aperture and increasing the possibility of describing the signal spread due to the interaction processes of the incoming photons. A completely new approach would be to use Monte Carlo methods to model the detector. This would increase the usefulness of such a program since the signal spread due to the interaction processes need not be known but could be simulated by the program. The proper introduction of noise sources would also increase the value of the program since this would lead to the possibility of simulating the DQE of the hypothetical systems.

- *Continuation of the work on two-dimensional representations of the imaging properties of digital radiographic systems.* This could be achieved both by applying the aperture mask method to different digital radiographic systems and by improving the validity of the method by including the low-frequency drop. The method should also be tested against the upcoming IEC standard for determining the one-dimensional DQE.

- *Investigation of different methods of obtaining the presampling MTF and DQE.* This would be useful in identifying the differences between the methods and in elucidating the reasons behind these differences.

The effects of anatomical structure on image quality have only been touched upon in this study. A great deal of work is needed to characterize these effects in detail. Little is known about how the overlaying of structures decreases the probability of detection and correct interpretation of a signal. One way to address the problem could be to use an inductive approach and investigate to what extent the background causes deterioration of the image quality for different combinations of pathological conditions and specific backgrounds. Regardless of the way in which the problem is finally solved, its solution is essential in the quest for the grand unification theory of radiography!

Acknowledgements

During the years I have spent on the work leading to this thesis I have received help from and been supported by colleagues, family and friends in many different ways. For this I am sincerely grateful since this thesis would otherwise not have come into being. I would especially like to express my warm gratitude to the following people.

My principal supervisor, Lars Gunnar Månsson; his critical thinking and scientific experience have been invaluable in this work. By always saying "What do you mean? Explain it to me!" he has forced me to transform fuzzy thoughts and vague ideas into, well, at least less fuzzy thoughts and less vague ideas.

My supervisor, Lars Jacobsson, as well as Eva Forssell-Aronsson, Head of the Department of Radiation Physics and Magne Alpsten, former Head of the Department of Radiation Physics, for pushing me in the right direction, showing interest in my work and giving an encouraging word when needed.

My colleagues and co-authors, Patrik Sund and Markus Håkansson; it is so much easier to accomplish a project like this with the help of a good friend. I have been fortunate enough to have two!

Susanne Kheddache, co-author, who has taken the time to describe radiography from the radiologist's perspective.

All members of the European research projects "Predictivity and Optimisation in Diagnostic Radiology" and "Unification of Physical and Clinical Requirements for Medical X-ray Imaging", and of the Swedish research project "Characterisation and Optimisation of Medical X-Ray Imaging Systems", for interesting discussions, pleasant meetings and stimulating collaboration.

Lena Björneld and Margareta Widell for collecting the clinical images used in this work, Anders Karlsson for writing the software used for the soft-copy evaluation of the images and Agneta Flinck, Bengt Gottfridsson and Ulf Tylén for evaluating the images.

The roommates I have had during the years; Sven Anders Benjegård, Petra Bergström, Agnetha Gustafsson, Charlotta Johanson, Håkan Mattsson, Anneli Schmitt and Ann Wikström, who have actually made most of my hours in front of the computer pleasant ones.

All my colleagues at the Department of Radiation Physics at Göteborg University and at the Department of Medical Physics and Biomedical Engineering at

Sahlgrenska University Hospital, for their help, advice, and pleasant company during the years; I would have liked to have mentioned all of you. However, I would especially like to thank Anne Thilander Klang and Jonas Söderberg for reading the manuscript of this thesis, Niclas Pettersson and Raine Vesanen for being especially helpful when theoretical or practical problems were encountered, Mats Johansson, Anders Kristensson and Jan Samuelsson for skilful mechanical work on the slit and the aperture masks, Sven-Bertil Orström and Lars Lindskog for help with malfunctioning equipment, Gunilla Adielsson and Maria Elsby for taking care of practical matters, Kerstin Lagerstrand for valuable comments on Paper I, Jonny Hansson for encouraging me to finish this thesis and, last but not least, my 'sister-in-arms' during our time as doctoral students, Anna Bäck, who has fought against anxiety and feelings of insecurity – so easily encountered as a doctoral student – with me. You made it! Now it's my turn…

Mari Lehtimäki, Kalevi Manninen and Vesa Varjonen at IMIX ADR Oy, Steen Olesen and Stig Svensson at Mediel AB, Ene Kivilo-Carlsson and Stefan Ohlsson at Agfa-Gevaert AB, Michael Reichart at Agfa-Gevaert in Germany and Peter Lazarz at Fujifilm Sverige AB, for providing information about the equipment used in this work.

Lars-Göran Norén, my physics teacher in upper secondary school, for introducing me to the field of medical physics.

Helen Sheppard and John Gulliver for correcting my English.

My beloved Ewa, and the rest of my family, for putting up with me, believing in me and giving me the support I needed. Hopefully, I will be able to shed the extra selfishness I have developed during the final months of this work and repay your sacrifices…

Financial support from the Commission of the European Communities, the Swedish Foundation for Strategic Research, the Swedish Radiation Protection Institute, the King Gustav V Jubilee Clinic Cancer Research Foundation and the Anna Ahrenberg Foundation is gratefully acknowledged.

References

[1] R. F. Mould, *A History of X-Rays and Radium*, IPC Building & Contract Journals Ltd., Sutton, (1980).

[2] International Commission on Radiological Protection, *ICRP Publication 60: 1990 Recommendations of the International Commission on Radiological Protection*, Annals of the ICRP Vol. 21 No. 1-3, Pergamon Press, Oxford (1991).

[3] M. L. Giger and K. Doi, "Investigation of basic imaging properties in digital radiography. 1. Modulation transfer function," *Med. Phys.* **11**, 287-295 (1984).

[4] H. Fujita, D.-Y. Tsai, T. Itoh, K. Doi, J. Morishita, K. Ueda and A. Ohtsuka, "A simple method for determining the modulation transfer function in digital radiography," *IEEE Trans. Med. Imaging* **11**, 34-39 (1992).

[5] M. J. Yaffe and J. A. Rowlands, "X-ray detectors for digital radiography," *Phys. Med. Biol.* **42**, 1-39 (1997).

[6] H. G. Chotas, J. T. Dobbins III and C. E. Ravin, "Principles of digital radiography with large-area, electronically readable detectors: A review of the basics," *Radiology* **210**, 595-599 (1999).

[7] A. R. Lakshmanan and K. G. Rajan, "Diagnostic X ray imaging using photostimulable luminescence phosphor: An emerging alternative to photographic film," *Radiat. Prot. Dosimetry* **55**, 247-255 (1994).

[8] M. Sonoda, M. Takano, J. Miyahara and H. Kato, "Computed radiography utilizing scanning laser stimulated luminescence," *Radiology* **148**, 833-838 (1983).

[9] J. A. Rowlands, "The physics of computed radiography," *Phys. Med. Biol.* **47**, R123-R166 (2002).

[10] W. Zhao, I. Blevis, S. Germann, J. A. Rowlands, D. Waechter and Z. Huang, "Digital radiology using active matrix readout of amorphous selenium: construction and evaluation of a prototype real-time detector," *Med. Phys.* **24**, 1834-1843 (1997).

[11] W. Zhao and J. A. Rowlands, "Digital radiology using active matrix readout of amorphous selenium: Theoretical analysis of detective quantum efficiency," *Med. Phys.* **24**, 1819-1833 (1997).

[12] J. H. Siewerdsen, L. E. Antonuk, Y. El-Mohri, J. Yorkston, W. Huang, J. M. Boudry and I. A. Cunningham, "Empirical and theoretical investigation of the noise performance of indirect detection, active matrix flat-panel imagers (AMFPIs) for diagnostic radiology," *Med. Phys.* **24**, 71-89 (1997).

[13] D. L. Lee, L. K. Cheung, B. Rodricks and G. F. Powell, "Improved imaging performance of a 14"×17" direct radiography system using a Se/TFT detector," in *Medical Imaging 1998: Physics of Medical Imaging,* John M. Boone, James T. Dobbins III, Editors, Proceedings of SPIE Vol. 3336, 14-23 (1998).

[14] A. Tsukamoto, S. Yamada, T. Tomisaki, M. Tanaka, T. Sakaguchi, H. Asahina, K. Suzuki and M. Ikeda, "Development and evaluation of a large-area selenium-based flat panel detector for real-time radiography and fluoroscopy," in *Medical Imaging 1999: Physics of Medical Imaging,* John M. Boone, James T. Dobbins III, Editors, Proceedings of SPIE Vol. 3659, 14-23 (1999).

[15] O. Tousignant, M. Choquette, Y. Demers, L. Laperrière, J. Leboeuf, M. Honda, M. Nishiki, A. Takahashi and A. Tsukamoto, "Progress report on the performance of real time selenium flat panel detectors for direct X-ray imaging" in *Medical Imaging 2002: Physics of Medical Imaging,* Larry E. Antonuk, Martin J. Yaffe, Editors, Proceedings of SPIE Vol. 4682, 503-510 (2002).

[16] R. A. Street, J. T. Rahn, S. E. Ready, K. Shah, P. R. Bennett, Y. Dmitriyev, P. Mei, J.-P. Lu, R. B. Apte, J. Ho, K. Van Schuylenbergh, F. Lemmi, J. B. Boyce and P. Nylen, "X-ray imaging using lead iodide as a semiconductor detector," in *Medical Imaging 1999: Physics of Medical Imaging,* John M. Boone, James T. Dobbins III, Editors, Proceedings of SPIE Vol. 3659, 36-47 (1999).

[17] R. A. Street, M. Mulato, M. Schieber, H. Hermon, K. Shah, P. Bennett, Y. Dmitryev, J. Ho, R. Lau, E. Meerson, S. E. Ready, B. Reisman, Y. Sado, K. Van Schuylenbergh, A. Vilensky and A. Zuck, "Comparative study of PbI_2 and HgI_2 as direct detector materials for high resolution X-ray image sensors," in *Medical Imaging 2001: Physics of Medical Imaging,* Larry E. Antonuk, Martin J. Yaffe, Editors, Proceedings of SPIE Vol. 4320, 1-12 (2001).

[18] S. Adachi, N. Hori, K. Sato, S. Tokuda, T. Sato, K. Uehara, Y. Izumi, H. Nagata, Y. Yoshimura and S. Yamada, "Experimental evaluation of a-Se and CdTe flat-panel X-ray detectors for digital radiography and fluoroscopy," in *Medical Imaging 2000: Physics of Medical Imaging,* James T. Dobbins, John M. Boone, Editors, Proceedings of SPIE Vol. 3977, 38-47 (2000).

[19] S. Tokuda, H. Kishihara, S. Adachi, T. Sato, Y. Izumi, O. Teranuma, Y. Yamane and S. Yamada, "Large area deposition of poly-crystalline CdZnTe film and its applicability to X-ray panel detectors with superior sensitivity," in *Medical Imaging 2002: Physics of Medical Imaging,* Larry E. Antonuk, Martin J. Yaffe, Editors, Proceedings of SPIE Vol. 4682, 30-41 (2002).

[20] T. Ducourant, M. Michel, G. Vieux, T. Peppler, J. C. Trochet, R. F. Schulz, R. Bastiaens and F. Busse, "Optimization of key building blocks for a large area radiographic and fluoroscopic dynamic digital X-ray detector based on a-Si:H/CsI:Tl flat panel technology," in *Medical Imaging 2000: Physics of Medical Imaging,* John M. Boone, James T. Dobbins III, Editors, Proceedings of SPIE Vol. 3977, (2000).

[21] P. Granfors, "Characteristics of an amorphous silicon flat panel X-ray imaging detector," in *Medical Imaging 1999: Physics of Medical Imaging,* John M. Boone, James T. Dobbins III, Editors, Proceedings of SPIE Vol. 3659, 480-490 (1999).

[22] D. P. Trauernicht and J. Yorkston, "Screen design for flat-panel imagers in diagnostic radiology," in *Medical Imaging 1998: Physics of Medical Imaging,* John M. Boone, James T. Dobbins III, Editors, Proceedings of SPIE Vol. 3336, 477-484 (1998).

[23] P. Sund, L. G. Månsson, S. Kheddache, R. R. Norrlund, U. Tylén, L. Björneld and M. Widell, "Evaluation of soft-copy reporting for three digital systems for chest imaging using the new European quality criteria," *Radiat. Prot. Dosimetry* **90**, 189-192 (2000).

[24] S. Thunberg, H. Sklebitz, B. Ekdahl, L. Bätz, A. Lundin, H. Möller, F. Fleischmann, G. Kreider and T. Weidner, "OPDIMA: Large-area CCD-based X-ray image sensor for spot imaging and biopsy control in mammography" in *Medical Imaging 1999: Physics of Medical Imaging,* John M. Boone, James T. Dobbins III, Editors, Proceedings of SPIE Vol. 3659, 150-158 (1999).

[25] J. A. Rowlands, and J. Yorkston, "Flat panel detectors for digital radiography," in *Handbook of Medical Imaging. Volume 1. Physics and Psychophysics,* J. Beutel, H. L. Kundel, R. L. Van Metter, Editors, 223-328, Bellingham, SPIE Press (2000).

[26] S. Hejazi and D. P. Trauernicht, "System considerations in CCD-based X-ray imaging for digital chest radiography and digital mammography," *Med. Phys.* **24**, 287-297 (1997).

[27] A. D. Maidment and M. J. Yaffe, "Analysis of the spatial-frequency-dependent DQE of optically coupled digital mammography detectors," *Med. Phys.* **21**, 721-729 (1994).

[28] M. B. Williams, P. U. Simoni, L. Smilowitz, M. Stanton, W. Phillips and A. Stewart, "Analysis of the detective quantum efficiency of a developmental detector for digital mammography," *Med. Phys.* **26**, 2273-2285 (1999).

[29] I. A. Cunningham, "Applied linear-systems theory," in *Handbook of Medical Imaging. Volume 1. Physics and Psychophysics,* J. Beutel, H. L. Kundel, R. L. Van Metter, Editors, 79-159, Bellingham, SPIE Press (2000).

[30] W. Hillen, U. Schiebel and T. Zaengel, "Imaging performance of a digital storage phosphor system," *Med. Phys.* **14**, 744-751 (1987).

[31] H. Fujita, K. Ueda, J. Morishita, T. Fujikawa, A. Ohtsuka and T. Sai, "Basic imaging properties of a computed radiographic system with photostimulable phosphors," *Med. Phys.* **16**, 52-59 (1989).

[32] A. Workman, A. R. Cowen and D. S. Brettle, "Physical evaluation of computed radiography as a mammographic X-ray imaging system," *Br. J. Radiol.* **67**, 988-996 (1994).

[33] J. T. Dobbins III, D. L. Ergun, L. Rutz, D. A. Hinshaw, H. Blume and D. C. Clark, "DQE(f) of four generations of computed radiography acquisition devices," *Med. Phys.* **22**, 1581-1593 (1995).

[34] A. Workman and A. R. Cowen, "Improved image quality utilizing dual plate computed radiography," *Br. J. Radiol.* **68**, 182-188 (1995).

[35] E. Samei and M. J. Flynn, "Physical measures of image quality in photostimulable phosphor radiographic systems," in *Medical Imaging 1997: Physics of Medical Imaging,* Richard L. Van Metter, Jacob Beutel, Editors, Proceedings of SPIE Vol. 3032, 328-338 (1997).

[36] S. M. Kengyelics, J. H. Launders and A. R. Cowen, "Physical imaging performance of a compact computed radiography acquisition device," *Med. Phys.* **25**, 354-360 (1998).

[37] S. M. Kengyelics, A. G. Davies and A. R. Cowen, "A comparison of the physical imaging properties of Fuji ST-V, ST-VA, and ST-VN computed radiography image plates," *Med. Phys.* **25**, 2163-2169 (1998).

[38] C. D. Bradford, W. W. Peppler and J. T. Dobbins III, "Performance characteristics of a Kodak computed radiography system," *Med. Phys.* **26**, 27-37 (1999).

[39] K. A. Fetterly and N. J. Hangiandreou, "Image quality evaluation of a desktop computed radiography system," *Med. Phys.* **27**, 2669-2679 (2000).

[40] Y. Nakano, T. Gido, S. Honda, A. Maezawa, H. Wakamatsu and T. Yanagita, "Improved computed radiography image quality from a BaFI:Eu photostimulable phosphor plate," *Med. Phys.* **29**, 592-597 (2002).

[41] E. Samei and M. J. Flynn, "An experimental comparison of detector performance for computed radiography systems," *Med. Phys.* **29**, 447-459 (2002).

[42] D. L. Lee, L. K. Cheung, L. S. Jeromin, E. F. Palecki and B. Rodricks, "Radiographic imaging characteristics of a direct conversion detector using selenium and thin film transistor array," in *Medical Imaging 1997: Physics of Medical Imaging*, Richard L. Van Metter, Jacob Beutel, Editors, Proceedings of SPIE Vol. 3032, 88-96 (1997).

[43] S. M. Kengyelics, A. R. Cowen and A. G. Davies, "Image quality evaluation of a direct digital radiography detector operating in a UK radiology department", in *Medical Imaging 1999: Physics of Medical Imaging*, John M. Boone, James T. Dobbins III, Editors, Proceedings of SPIE Vol. 3659, 24-35 (1999).

[44] P. R. Granfors and R. Aufrichtig, "Performance of a 41×41-cm^2 amorphous silicon flat panel X-ray detector for radiographic imaging appplications," *Med. Phys.* **27**, 1324-1331 (2000).

[45] E. Samei, M. J. Flynn, H. G. Chotas and J. T. Dobbins III, "DQE of direct and indirect digital radiography systems," in *Medical Imaging 2001: Physics of Medical Imaging,* Larry E. Antonuk, Martin J. Yaffe, Editors, Proceedings of SPIE Vol. 4320, 189-197 (2001).

[46] E. Samei and M. J. Flynn, "An experimental comparison of detector performance for for direct and indirect digital radiography systems," *Med. Phys.* **30**, 608-622 (2003).

[47] R. Fahrig, J. A. Rowlands and M. J. Yaffe, "X-ray imaging with amorphous selenium: detective quantum efficiency of photoconductive receptors for digital mammography," *Med. Phys.* **22**, 153-160 (1995).

[48] L. E. Antonuk, Y. El-Mohri, K.-W. Jee, M. Maolinbay, S. C. Nassif, X. Rong, J. H. Siewerdsen and Q. Zhao, "Beyond the limits of present active matrix, flat-panel imagers (AMFPIs) for diagnostic radiology," in *Medical Imaging 1999: Physics of Medical Imaging*, John M. Boone, James T. Dobbins III, Editors, Proceedings of SPIE Vol. 3659, 518-527 (1999).

[49] W. K. Leitz, L. G. Månsson, B. R. K. Hedberg-Vikström and S. Kheddache, "In search of optimum chest radiography techniques," *Br. J. Radiol.* **66**, 314-321 (1993).

[50] B. Lanhede, A. Tingberg, L. G. Månsson, S. Kheddache, M. Widell, L. Björneld, P. Sund, A. Almén, J. Besjakov, S. Mattsson, M. Zankl, W. Panzer and C. Herrmann, "The influence of different technique factors on image quality for chest radiographs: Application of the recent CEC image quality criteria," *Radiat. Prot. Dosimetry* **90**, 203-206 (2000).

[51] A. Tingberg, C. Herrmann, B. Lanhede, A. Almén, J. Besjakov, S. Mattsson, P. Sund, S. Kheddache and L. G. Månsson, "Comparison of two methods for evaluation of the image quality of lumbar spine radiographs," *Radiat. Prot. Dosimetry* **90**, 165-168 (2000).

[52] A. Almén, A. Tingberg, S. Mattsson, J. Besjakov, S. Kheddache, B. Lanhede, L. G. Månsson and M. Zankl, "The influence of different technique factors on image quality of lumbar spine radiographs as evaluated by established CEC image criteria," *Br. J. Radiol.* **73**, 1192-1199 (2000).

[53] B. Axelsson, U. Petersen and H. J. Wiltz, "Reduction of absorbed dose by adaptation of exposure factors and image processing," *Acta Radiol.* **42**, 592-598 (2001).

[54] L. G. Månsson, *Evaluation of Radiographic Procedures - Investigations Related to Chest Imaging*, Thesis, Göteborg University, Göteborg (1994).

[55] L. G. Månsson, "Methods for the evaluation of image quality: a review," *Radiat. Prot. Dosimetry* **90**, 89-99 (2000).

[56] J. A. Swets and R. M. Picket, *Evaluation of Diagnostic Systems - Methods from Signal Detection Theory*, Academic Press, New York (1982).

[57] C. E. Metz, "ROC methodology in radiologic imaging," *Invest. Radiol.* **21**, 720-733 (1986).

[58] R. G. Swensson, "Unified measurement of observer performance in detecting and localizing target objects on images," *Med. Phys.* **23**, 1709-1725 (1996).

[59] C. E. Metz, "Fundamental ROC analysis," in *Handbook of Medical Imaging. Volume 1. Physics and Psychophysics,* J. Beutel, H. L. Kundel, R. L. Van Metter, Editors, 751-769, Bellingham, SPIE Press (2000).

[60] K. J. Myers, "Ideal observer models of visual signal detection," in *Handbook of Medical Imaging. Volume 1. Physics and Psychophysics,* J. Beutel, H. L. Kundel, R. L. Van Metter, Editors, 559-592, Bellingham, SPIE Press (2000).

[61] M. P. Eckstein, C. K. Abbey and F. O. Bochud, "A practical guide to model observers for visual detection in synthetic and natural noisy images," in *Handbook of Medical Imaging. Volume 1. Physics and Psychophysics,* J. Beutel, H. L. Kundel, R. L. Van Metter, Editors, 593-628, Bellingham, SPIE Press (2000).

[62] C. K. Abbey and F. O. Bochud, "Modeling visual detection tasks in correlated image noise with linear model observers," in *Handbook of Medical Imaging. Volume 1. Physics and Psychophysics,* J. Beutel, H. L. Kundel, R. L. Van Metter, Editors, 629-654, Bellingham, SPIE Press (2000).

[63] J. C. Dainty and R. Shaw, *Image science – Principles, Analysis and Evaluation of Photographic-Type Imaging Processes*, Academic Press, London (1974).

[64] J. F. James, *A Student's Guide to Fourier Transforms – With Applications in Physics and Engineering,* Cambridge University Press, New York (1995).

[65] J. T. Dobbins III, "Effects of undersampling on the proper interpretation of modulation transfer function, noise power spectra, and noise equivalent quanta of digital imaging systems," *Med. Phys.* **22**, 171-181 (1995).

[66] J. T. Dobbins III, "Image quality metrics for digital systems," in *Handbook of Medical Imaging. Volume 1. Physics and Psychophysics,* J. Beutel, H. L. Kundel, R. L. Van Metter, Editors, 161-222, Bellingham, SPIE Press (2000).

[67] H. Fujita, M. L. Giger and K. Doi, "Investigation of basic imaging properties in digital radiography. 12. Effect of matrix configuration on spatial resolution," *Med. Phys.* **15**, 384-390 (1988).

[68] G. K. Sanderson, "Imaging assessment: LSF and MTF," in *The Physics of Medical Imaging – Recording System Measurements and Techniques,* A. G. Haus, Editor, 118-137, American Institute of Physics, Inc., New York (1979).

[69] G. T. Barnes, "The use of bar pattern test objects in assessing the resolution of film/screen systems," in *The Physics of Medical Imaging – Recording System Measurements and Techniques,* A. G. Haus, Editor, 138-151, American Institute of Physics, Inc., New York (1979).

[70] I. A. Cunningham and B. K. Reid, "Signal and noise in modulation transfer function determinations using the slit, wire, and edge techniques," *Med. Phys.* **19**, 1037-1044 (1992).

[71] C. D. Bradford, W. W. Peppler and J. M. Waidelich, "Use of a slit camera for MTF measurements," *Med. Phys.* **26**, 2286-2294 (1999).

[72] I. A. Cunningham and A. Fenster, "A method for modulation transfer function determination from edge profiles with correction for finite-element differentiation," *Med. Phys.* **14**, 533-537 (1987).

[73] E. Samei, M. J. Flynn and D. A. Reimann, "A method for measuring the presampled MTF of digital radiographic systems using an edge test device," *Med. Phys.* **22**, 102-113 (1998).

[74] J. Morishita, K. Doi, R. Bollen, P. C. Bunch, D. Hoeschen, G. Sirand-rey and Y. Sukenobu, "Comparison of two methods for accurate measurement of modulation transfer functions of screen-film systems," *Med. Phys.* **22**, 193-200 (1995).

[75] S.-Å. Starck and S. Carlsson, "A phantom for the measurement of transfer functions in nuclear medicine image processing," *Radiat. Prot. Dosimetry* **49**, 303-305 (1993).

[76] T. A. Hander, J. L. Lancaster, D. T. Kopp, J. C. Lasher, R. Blumhardt and P. T. Fox, "Rapid objective measurement of gamma camera resolution using statistical moments," *Med. Phys.* **24**, 327-334 (1997).

[77] J. M. Boone, "Determination of the presampled MTF in computed tomography," *Med. Phys.* **28**, 356-360 (2001).

[78] M. C. Steckner, D. J. Drost and F. S. Prato, "Computing the modulation transfer function of a magnetic resonance imager," *Med. Phys.* **21**, 483-489 (1994).

[79] J.-P. Bissonnette, I. A. Cunningham and P. Munro, "Optimal phosphor thickness for portal imaging," *Med. Phys.* **24**, 803-814 (1997).

[80] T. Falco and B. G. Fallone, "Characteristics of metal-plate/film detectors at therapy energies. I. Modulation transfer function," *Med. Phys.* **25**, 2455-2462 (1998).

[81] P. J. Papin and H. K. Huang, "A prototype amorphous selenium imaging plate system for digital radiography," *Med. Phys.* **14**, 322-329 (1987).

[82] R. A. Sones and G. T. Barnes, "A method to measure the MTF of digital X-ray systems," *Med. Phys.* **11**, 166-171 (1984).

[83] H. Fujita, K. Doi and M. L. Giger, "Investigation of basic imaging properties in digital radiography. 6. MTFs of II-TV digital imaging systems," *Med. Phys.* **12**, 713-720 (1985).

[84] K. Stierstorfer and M. Spahn, "Self-normalizing method to measure the detective quantum efficiency of a wide range of X-ray detectors," *Med. Phys.* **26**, 1312-1319 (1999).

[85] P. B. Greer and T. van Doom, "Evaluation of an algorithm for the assessment of the MTF using an edge method," *Med. Phys.* **27**, 2048-2059 (2000).

[86] D. A. Hinshaw and J. T. Dobbins III, "Plate scatter correction for improved performance in dual-energy imaging," *Med. Phys.* **23**, 871-876 (1996).

[87] K. A. Fetterly and N. J. Hangiandreou, "Effects of X-ray spectra on the DQE of a computed radiography system," *Med. Phys.* **28**, 241-249 (2001).

[88] F.-F. Yin, M. L. Giger and K. Doi, "Measurement of the presampling modulation transfer function of film digitizers using a curve fitting technique," *Med. Phys.* **17**, 962-966 (1990).

[89] J. M. Boone, T. Yu and J. A. Seibert, "Sinusoidal modulation analysis for optical system MTF measurements," *Med. Phys.* **23**, 1955-1963 (1996).

[90] T. Yu, J. M. Sabol, J. A. Seibert and J. M. Boone, "Scintillating fiber optics screens: A comparison of MTF, light conversion efficiency, and emission angle with Gd_2O_2S:Tb screens," *Med. Phys.* **24**, 279-285 (1997).

[91] D. A. Reimann, H. A. Jacobs and E. Samei, "Use of Wiener filtering in the measurement of the two-dimensional modulation transfer function," in *Medical Imaging 2000: Physics of Medical Imaging*, James T. Dobbins III, John M. Boone, Editors, Proceedings of SPIE Vol. 3977, 670-680 (2000).

[92] M. L. Giger, K. Doi and C. E. Metz, "Investigation of basic imaging properties in digital radiography. 2. Noise Wiener spectrum," *Med. Phys.* **11**, 797-805 (1984).

[93] R. Aufrichtig, Y. Su, Y. Cheng and P. R. Granfors, "Measurement of the noise power spectrum in digital X-ray detectors," in *Medical Imaging 2001: Physics of Medical Imaging*, Larry E. Antonuk, Martin J. Yaffe, Editors, Proceedings of SPIE Vol. 4320, 362-372 (2001).

[94] U. Neitzel, I. Maack and S. Gunther Kohfahl, "Image quality of a digital chest radiography system based on a selenium detector," *Med. Phys.* **21**, 509-516 (1994).

[95] J. H. Siewerdsen, L. E. Antonuk, Y. El-Mohri, J. Yorkston, W. Huang and I. A. Cunningham, "Signal, noise power spectrum, and detective quantum efficiency of indirect-detection flat-panel imagers for diagnostic radiology," *Med. Phys.* **25**, 614-628 (1998).

[96] M. J. Flynn and E. Samei, "Experimental comparison of noise and resolution for 2*k* and 4*k* storage phosphor radiography systems," *Med. Phys.* **26**, 1612-1623 (1999).

[97] C. E. Metz, R. F. Wagner, K. Doi, D. G. Brown, R. M. Nishikawa and K. J. Myers, "Toward consensus on quantitative assessment of medical imaging systems," *Med. Phys.* **22**, 1057-1061 (1995).

[98] J. M. Sandrik and R. F. Wagner, "Absolute measures of physical image quality: Measurement and application to radiographic magnification," *Med. Phys.* **9**, 540-549 (1982).

[99] International Commission on Radiation Units and Measurements, *ICRU Report 54: Medical Imaging – The Assessment of Image Quality*, International Commission on Radiation Units and Measurements, Bethesda (1996).

[100] M. J. Tapiovaara and R. F. Wagner, "SNR and DQE analysis of broad spectrum X-ray imaging," *Phys. Med. Biol.* **30**, 519-529 (1985).

[101] M. Sandborg and G. Alm Carlsson, "Influence of X-ray energy spectrum, contrasting detail and detector on the signal-to-noise ratio (SNR) and detective quantum efficiency (DQE) in projection radiography," *Phys. Med. Biol.* **37**, 1245-1263 (1992).

[102] R. N. Cahn, B. Cederström, M. Danielsson, A. Hall, M. Lundqvist and D. Nygren, "Detective quantum efficiency dependence on X-ray energy weighting in mammography," *Med. Phys.* **26**, 2680-2683 (1999).

[103] The Institute of Physics and Engineering in Medicine, *IPEM Report No. 78: Catalogue of Diagnostic X-Ray Spectra & Other Data*, The Institute of Physics and Engineering in Medicine, York (1997). CD-ROM

[104] J. P. Moy, "Signal-to-noise ratio and spatial resolution in X-ray electronic imagers: is the MTF a relevant parameter?," *Med. Phys.* **27**, 86-93 (2000).

[105] R. M. Nishikawa, M. J. Yaffe and R. B. Holmes, "Effect of finite phosphor thickness on detective quantum efficiency," *Med. Phys.* **16**, 773-780 (1989).

[106] R. M. Nishikawa and M. J. Yaffe, "Effect of various noise sources on the detective quantum efficiency of phosphor screens," *Med. Phys.* **17**, 887-893 (1990).

[107] R. M. Nishikawa and M. J. Yaffe, "Model of the spatial-frequency-dependent detective quantum efficiency of phosphor screens," *Med. Phys.* **17**, 894-904 (1990).

[108] I. A. Cunningham, M. S. Westmore and A. Fenster, "A spatial-frequency dependent quantum accounting diagram and detective quantum efficiency model of signal and noise propagation in cascaded imaging systems," *Med. Phys.* **21**, 417-427 (1994).

[109] I. A. Cunningham, M. S. Westmore and A. Fenster, "Visual impact of the non-zero spatial frequency quantum sink," in *Medical Imaging 1994: Physics of Medical Imaging*, Rodney Shaw, Editor, Proceedings of SPIE Vol. 2163, 274-283 (1994).

[110] W. Que and J. A. Rowlands, "X-ray imaging using amorphous selenium: Inherent spatial resolution," *Med. Phys.* **22**, 365-374 (1995).

[111] I. A. Cunningham, "Degradation of the detective quantum efficiency due to a non-unity detector fill factor," in *Medical Imaging 1997: Physics of Medical Imaging*, Richard L. van Metter, Jacob Beutel, Editors, Proceedings of SPIE Vol. 3032, 22-31 (1997).

[112] W. G. Ji, W. Zhao and J. A. Rowlands, "Digital X-ray imaging using amorphous selenium: Reduction of aliasing," *Med. Phys.* **25**, 2148-2162 (1998).

[113] I. A. Cunningham and R. Shaw, "Signal-to-noise optimization of medical imaging systems," *J. Opt. Soc. Am.* **16**, 621-632 (1999).

[114] W. Zhao, W. G. Ji and J. A. Rowlands, "Effects of characteristic x rays on the noise power spectra and detective quantum efficiency of photoconductive X-ray detectors," *Med. Phys.* **28**, 2039-2049 (2001).

[115] J. G. Mainprize, D. C. Hunt and M. J. Yaffe, "Direct conversion detectors: The effect of incomplete charge collection on detective quantum efficiency," *Med. Phys.* **29**, 976-990 (2002).

[116] E. Hecht, *Optics* (2nd ed.), Addison-Wesley Publishing Company, Inc., Reading, (1987).

[117] K. A. Fetterly, N. J. Hangiandreou, B. A. Schueler and E. R. Ritenour, "Measurement of the presampled two-dimensional modulation transfer function of digital imaging systems," *Med. Phys.* **29**, 913-921 (2002).

[118] M. Albert and A. D. A. Maidment, "Linear response theory for detectors consisting of discrete arrays," *Med. Phys.* **27**, 2417-2434 (2000).

[119] F. R. Verdun, F. Bochud, C. Depeursinge, L. Desponds, M. Grecescu, C. Hessler, S. Raimondi and J.-F. Valley, "Subjective and objective evaluation of chest imaging systems," *Radiat. Prot. Dosimetry* **49**, 91-94 (1993).

[120] A. E. Burgess, F. L. Jacobson and P. F. Judy, "Human observer detection experiments with mammograms and power-law noise," *Med. Phys.* **28**, 419-437 (2001).

[121] E. Samei, M. J. Flynn and W. R. Eyler, "Detection of subtle lung nodules: relative influence of quantum and anatomic noise on chest radiographs," *Radiology* **213**, 727-734 (1999).

[122] E. Samei, W. Eyler and L. Baron, "Effects of anatomical structure on signal detection," in *Handbook of Medical Imaging. Volume 1. Physics and Psychophysics*, J. Beutel, H. L. Kundel, R. L. Van Metter, Editors, 655-682, Bellingham, SPIE Press (2000).

[123] A. Tingberg, *Quantifying the Quality of Medical X-Ray Images - An Evaluation Based on Normal Anatomy for Lumbar Spine and Chest Images*, Thesis, Lund University, Lund (2000).

[124] H. Geijer, B. Verdonck, K.-W. Beckman, T. Andersson and J. Persliden, "Digital radiography of scoliosis with a scanning method: initial evaluation," *Radiology* **218**, 402-410 (2001).

[125] K. C. Young and M. L. Ramsdale, "Evaluation of mammography image quality phantoms," *Radiat. Prot. Dosimetry* **49**, 171-173 (1993).

[126] H. M. Olerud, J. B. Olsen, A. Widmark and H. Fosmark, "A Norwegian survey of image quality, doses and film processing in mammography, with reference to two technical phantoms," *Radiat. Prot. Dosimetry* **67**, 199-210 (1996).

[127] S. Kheddache and H. Kvist, "Digital mammography using a storage phosphor plate technique - optimizing image processing parameters for the visibility of lesions and anatomy," *Eur. J. Radiol.* **24**, 237-244 (1997).

[128] H. Seifert, H.-J. Jesberger, G. Schneider, L. Rein, G. Blass, H.-G. Limbach, M. Niewald, F. C. Sitzmann and B. Kramann, "Dose reduction in thorax radiography in simulated neonates with additional filtration and digital luminescence radiography," *Acta Radiol.* **39**, 514-519 (1998).

[129] M. Sandborg, G. McVey, D. R. Dance and G. Alm Carlsson, "Comparison of model predictions of image quality with results of clinical trials in chest and lumbar spine screen-film imaging," *Radiat. Prot. Dosimetry* **90**, 173-176 (2000).

[130] P. Sund, M. Båth, S. Kheddache, U. Tylén and L. G. Månsson, "Evaluation of image quality of a new CCD-based system for chest imaging," in *Medical Imaging 2000: Physics of Medical Imaging*, James T. Dobbins III, John M. Boone, Editors, Proceedings of SPIE Vol. 3977, 437-444 (2000).

[131] P. Sund, C. Herrmann, A. Tingberg, S. Kheddache, L. G. Månsson, A. Almén and S. Mattsson, "Comparison of two methods for evaluating image quality of chest radiographs," in *Medical Imaging 2000: Image Perception and Performance*, Elizabeth A. Krupinski, Editor, Proceedings of SPIE Vol. 3981, 251-257 (2000).

[132] A. Tingberg, C. Herrmann, J. Besjakov, K. Rodenacker, A. Almén, P. Sund, S. Mattsson and L. G. Månsson, "Evaluation of lumbar spine images with added pathology," in *Medical Imaging 2000: Image Perception and Performance*, Elizabeth A. Krupinski, Editor, Proceedings of SPIE Vol. 3981, 34-42 (2000).

[133] M. Sandborg, A. Tingberg, D. R. Dance, B. Lanhede, A. Almén, G. McVey, P. Sund, S. Kheddache, J. Besjakov, S. Mattsson, L. G. Månsson and G. Alm Carlsson, "Demonstration of correlations between clinical and physical image quality measures in chest and lumbar spine screen-film radiography," *Br. J. Radiol.* **74**, 520-528 (2001).

[134] P. C. Brennan and S. A. Devereux, "An assessment of the usefulness of screen-film speed classifications," *Eur. Radiol.* **12**, 1577-1583 (2002).

[135] B. Lanhede, M. Båth, S. Kheddache, P. Sund, L. Björneld, M. Widell, A. Almén, J. Besjakov, S. Mattsson, A. Tingberg, C. Herrmann, W. Panzer, M. Zankl and L. G. Månsson, "The influence of different technique factors on image quality of chest radiographs as evaluated by modified CEC image quality criteria," *Br. J. Radiol.* **75**, 38-49 (2002).

[136] P. Sund, M. Håkansson, L. Lindskog, U. Tylén, S. Kheddache and L. G. Månsson, "Evaluation of displays for medical X-ray applications using observer performance," in *Medical Imaging 2002: Image Perception, Observer Performance, and Technology Assessment*, Dev P. Chakraborty, Elizabeth A. Krupinski, Editors, Proceedings of SPIE Vol. 4686, 139-144 (2002).

[137] European Commission, *EUR 16260 – European Guidelines on Quality Criteria for Diagnostic Radiographic Images*, Office for Official Publications of the European Communities, Luxembourg (1996).

[138] European Commission, *EUR 16261 – European Guidelines on Quality Criteria for Diagnostic Radiographic Images in Paediatrics,* Office for Official Publications of the European Communities, Luxembourg (1996).

[139] European Commission, *EUR 16262 – European Guidelines on Quality Criteria for Computed Tomography*, Office for Official Publications of the European Communities, Luxembourg (1996).

[140] D. P. Chakraborty and L. H. L. Winter, "Free-response methodology: alternate analysis and a new observer-performance experiment," *Radiology* **174**, 873-881 (1990).

[141] D. G. Altman, *Practical Statistics for Medical Research*, Chapman&Hall, London (1991).

På grund av upphovsrättsliga skäl kan vissa ingående delarbeten ej publiceras här.
För en fullständig lista av ingående delarbeten, se avhandlingens början.

Due to copyright law limitations, certain papers may not be published here.
For a complete list of papers, see the beginning of the dissertation.

GÖTEBORGS UNIVERSITET
GÖTEBORGS UNIVERSITETSBIBLIOTEK

MILJÖMÄRKT

Digitaltryckt & Bunden
Vasastadens Bokbinderi AB
Göteborg 2003

GÖTEBORG
UNIVERSITY

Faculty of Science

ISBN 91-628-5651-0